INVESTIGATION OF THE PREPARATION OF MATERIALS IN SPACE

TASK IV

FIELD MANAGEMENT FOR WEIGHTLESS CONTAINERLESS PROCESSING

By

R. T. Frost
A. Gatti
H. Halsey
L. McCreight
L. Napaluch
E. Stockhoff
G. Wouch

Second Quarterly Progress Report
Covering the Period 22 August 1969 – 31 October 1969

Contract No. NAS 8-24683
Modification No. 2

Control No. DCN 1-9-54-20055, S2

Prepared for

NATIONAL AERONAUTICS AND SPACE ADMINISTRATION
MANUFACTURING ENGINEERING LABORATORY
MARSHALL SPACE FLIGHT CENTER

November 15, 1969

Space Sciences Laboratory
GENERAL ELECTRIC COMPANY
P. O. BOX 8555
Philadelphia, Pennsylvania 19101

INVESTIGATION OF THE PREPARATION OF MATERIALS IN SPACE

TASK IV

FIELD MANAGEMENT FOR WEIGHTLESS CONTAINERLESS PROCESSING

By

R. T. Frost
A. Gatti
H. Halsey
L. McCreight
L. Napaluch
E. Stockhoff
G. Wouch

Second Quarterly Progress Report
Covering the Period 22 August 1969 – 31 October 1969

Contract No. NAS 8-24683
Modification No. 2

Control No. DCN 1-9-54-20055, S2

Prepared for

NATIONAL AERONAUTICS AND SPACE ADMINISTRATION
MANUFACTURING ENGINEERING LABORATORY
MARSHALL SPACE FLIGHT CENTER

November 15, 1969

Space Sciences Laboratory
GENERAL ELECTRIC COMPANY
P. O. BOX 8555
Philadelphia, Pennsylvania 19101

FOREWORD

The second quarterly report describes the efforts during the period 22 August 1969 – 31 October 1969 on Task IV of contract NAS 8-24683. The first three tasks under this contract are concerned with the collection and assessment of ideas for the exploitation of the space environment. These tasks are especially concerned with:

I. Growth of high density, highly perfect crystals

II. Melting, purification and solidification of materials

III. Unit separation processes.

Work on these first three tasks is monitored by Dr. E. C. McKannon, Marshall Space Flight Center, and is reported separately. The work reported herein is concerned with a 4th Task and is monitored by Leroy H. Berge, Marshall Space Flight Center. This work has as its objective the definition in some depth of the physical problems associated with the melting, purification and solidification of free floating materials in a weightless environment. Another objective of this Task is to define experimental techniques and hardware which will be required in developing new metallurgical and ceramic processes for exploitation of the space environment.

TABLE OF CONTENTS

I. SUMMARY

During the first quarter some work was done on most of the tasks specified in the RFP. Most intensive work was concentrated on reviewing and extending the theory of electromagnetic position control for a freely floating, conducting sphere and the implementation of initial experiments on position control.

Techniques were developed for measurement of small forces on conducting spheres suspended alternately on a long pendulum or freely rolling on a precision glass tilt table. Force measurements under a variety of conditions were compared with theory. Stability of the suspended mass in two dimensions was demonstrated without the use of position sensing or control.

An electronic servo was designed, constructed and demonstrated to be capable of high accuracy position sensing for rapid damping of position and position rate errors.

Some work was begun on general considerations to study the range of applicability for electromagnetic or electrostatic positioning of materials having a wide range of properties. Work was also begun to define associated hydrodynamic problems concerned with creation or damping of shape oscillations and generation of fluid currents for mixing or shape control.

Work was contributed by the Materials Research and Development Section towards a survey of candidate metallurgical and ceramic processes for weightless space processing.

A paper was presented to the NASA symposium on Space Processing and Manufacturing consisting of a short summary of the work described herein.

II. PROGRAM STATUS

A considerable effort was expended during the first quarter to provide experimental hardware which will be needed for experiments during the remainder of the program and to obtain some early experimental results and theoretical calculations for presentation at the NASA symposium which was held in October.

A. Study of Example Metallurgical and Ceramic Processes for Zero Gravity (Contributors: A. Gatti, M. Noone)

Visits were made to the General Electric Research and Development Center in Schenectady on two occasions. A visit to the Philadelphia Switchgear Operation and numerous telephone calls were made to provide material summarized in Section III of this report. During the next quarter it is planned to extend this work to the selection of processes most amenable to first space experiments for the purpose of initiating specific experiment proposals and for defining the characteristics and number of space processing chambers which should be considered.

B. Theory of Electromagnetic Position Control and Body Distributed Currents (Contributors: G. Wouch, E. Gray)

The work of Smythe was extended to include the magnetic field and body distributed forces within a conducting sphere. Computer programs were written and debugged giving the currents, fields and instantaneous as well as cyle average forces throughout a spherical conducing body immersed in a uniform oscillating magnetic field. Body force for position control as a function of ball position relative to a position control coil were evaluated. A number of graphs giving the theoretical solutions were prepared which are applicable to a wide range of material properties in terms of electric conductivity, frequency, and sphere radius. This was achieved by plotting the results in dimensionless form insofar as possible.

C. Force Measurements (Contributor: E. Stockhoff)

Apparatus was designed for position measurements, force measurements and positioning control experiments. Most of this work was carried out using either a balance technique or a pendulum suspension. Initial experiments were begun using a precision glass tilt table. Comparison was made between experimental and predicted force values and nonlinear addition of forces exerted by separate coils was observed qualitatively.

During the next quarter this apparatus will be used to establish force measurements to explore the domains of applicability of these techniques to poor conductors.

D. Position Sensing and Control Servo (Contributors: L. Napaluch, H. Halsey assisted by two wiremen

The servo apparatus was designed and constructed. The two-axis sensing and control servo consists of the following items:

1. Sensing and control coils
2. Position sensing logic circuitry
3. Error amplifiers
4. Modulators
5. Power amplifiers

During the next quarter it may be possible to make some improvements in the operation of the present circuits and to test applicability to poor conductors. The power amplifiers are capable of furnishing sufficient heat to melt low melting alloys. For this purpose a vertical levitation coil must be added to the present experiment. Quadrature phasing of coil pairs to effect sphere rotation is another possibility if remaining funding allows this.

E. Position Sensing and Control for Various Materials – General Considerations (Contributors: G. Wouch, E. Stockhoff)

Work in this area was only begun and is intended to survey the following regimes of material properties.

1. Skin depth
2. Ratio of conduction current to displacement current
3. Achievable position control force levels
4. Appropriatness of electromagnetic vs. electrostatic control for poor conductors
5. Power required for melting
6. Parameters affecting period and damping time for shape oscillations

This work will be guided, in so far as possible, by results discussed in paragraph A.

F. Hydrodynamics (Contributor: G. Wouch)

Work was barely started in this area and the results reported here are necessarily qualitative for the most part. Some of the problems which have been defined would require rather extensive computations for their solution. A Navier Stokes program is available in the Space Sciences Laboratory with boundary conditions treated in terms of flexible membranes. This may be applicable to our boundary conditions consisting of a surface tension pressure. It is also planned to carry out further discussions with the MSFC Computer Laboratory to determine whether they can assist in the solution of some of these hydrodynamic problems.

As a start some idealized flow problems must be defined and considered analytically. It is believed that adequate solutions for our purposes already exist in the case of shape oscillations. Excitation by electromagnetic magnetostrictive forces must be considered during the next quarter.

III. EXAMPLE METALLURGICAL AND CERAMIC PROCESSES FOR ZERO GRAVITY

A. General Classes of Phenomena for Exploitation of Weightlessness for Material Processing

Table III-1 lists four general areas of phenomena which can be considered to exploit the weightless state. The most obvious application is the elimination of buoyant segregation in multiphase systems where present forming techniques are limited by separation of phases of different densities. Materials of this type often must be prepared by powder metallurgy techniques which result in low ductility and creep resistance or which prevent molding into precision shapes.

TABLE III-1. POTENTIAL CRUCIBLELESS METALLURIGCAL/CERAMIC PROCESSES FOR ZERO-GRAVITY APPLICATIONS

Elimination of Buoyant Segregation

Precision Molding of Reactive and High Melting Metals

Formation of New Phase or Micro-Crystal Structure Thru Sub-Cooled Solidification

Prevention of Crystallization by Avoidance of Mold Contact

The second example refers to the new possibility of carrying out precision molding of reactive and high melting materials which presently must be prepared by skull melting techniques which do not allow for the provision of superheat. This severely limits the shapes which can be cast. In a free floating state superheat could be provided even for very reactive materials.

A more speculative possibility is the achieving of high degrees of subcooling prior to solidification because of absence of contact between the melt and any solid object. High degrees of subcooling have been observed in limited terrestrial levitation experiments and new crystal phases have been observed, such as Gallium III, to form at subcooled temperatures. Another possibility which has been suggested is the preparation of high refractive index glass where recrystallization due to mold contact is a present limitation.

B. Elimination of Buoyant Segregation

The lack of bouyancy inherent in space processing presents a unique opportunity to combine materials which have large density differences and are mutually insoluble. This is not to imply that only those systems which contain liquid phases are interesting; however, present problems involving this principle are most applicable to solid particle-liquid matrix systems which at one "g" can only

be processed by powder means and solid-state consolidation. Examples of commercial materials presently available which utilize these processing techniques are Ni–ThO_2, developed by duPont, and SAP (AL-Al_2O_3), developed by Ermann (1). It is to be noted that these present materials are both difficult and costly to process because of the necessity of the thermo-mechanical working of finely devided and intimately mixed oxide-metal powders. Final shaping of these relatively low-ductility, hard and strong materials is also costly. The expedient and inexpensive precision casting of such alloys in space presents an interesting and challenging application.

A prime example of a present-day critical problem is the oxidation-corrosion of high temperature super alloys in or near sea-air environments. Accelerated corrosion can limit jet engine life to 50–100 hour operation, mainly because present day blade and vane parts are cast materials of thin-walled design (0.050 in. thick sections) to allow air cooling and thus higher operating temperatures and greater efficiency.

Wasielewski (2), (3), (4) has extensively studied the oxidation/hot corrosion of superalloys and has documented the beneficial effects which the rare earth metals have on the hot corrosion process. Additions of Lanthanium and Cerium as metals, however, lead to low melting eutectics at grain boundaries, severely limiting the high temperature capabilities of the alloy. Through these initial efforts, it had been recognized that the rare earth oxides are the effective barrier rather than the metal itself. This developed from the observations that the rare earths were always oxidized preferentially by internal oxidation for a considerable depth within the surface of the super alloys. Work by Seybolt (5) and Allen (6) has further delineated these effects and has shown that the protection mechanism depends wholly on the presence of oxide and that the dispersion or size of the particle need not be critical. Accelerated corrosion occurs as a result of combining sodium with the sulfur in fuels to form Na_2So_4 which then rapidly depletes chromium from the matrix and carbide structure of super alloys at operating temperatures. The additon of rare earth oxides has a beneficial effect on the corrosion rate under these operating conditions and is represented by the simplified chemical equations shown in Figure III-1. Thus it was recognized that rare earth metallic additions were not necessary to impart oxidation/hot corrosion resistance but oxide additions were, with the possibility then of circumventing the eutectic problem.

Presently, because of the large difference in density between rare earth oxides and super alloy mixtures, only powder metallurgy techniques can be utilized to form oxide-metal dispersions. Figure III-2 is a dramatic demonstration of the oxidation/hot corrosion problem and the protective role which the rare earth oxides play. These two specimens of TRW-6A alloys (a modern super alloy developed by Thomson, Ramo, Woolrich) were fabricated from prealloyed powders, to which ½% by weight CeO_2 was added to the almost unaffected sample. These samples were initially ¼ in. diameter rods which were exposed to 1725°F for fifty hours with 100 ppm NaCl added to the intake gases. Present conservative estimates(5)are that rare earth additions to super alloys will more than double their useful life.

Modern super alloy parts are air cooled (contain air passages, are essentially hollow) must have maximum ductility and good thermal shock resistance. These requirements are met in severely alloyed materials only by casting methods which produce large grain sizes; single crystal parts are more desirable (7) but difficult and expensive to manufacture. Limitations on powder processing of super alloys with rare earth oxides can be characterized by their inherent fine grain size, and thus lower ductility, thermal shock susceptability and creep resistance.

The processing of such alloys in space gives the opportunity to combine the advantage of cast structures with the addition of dispersed rare earth oxides to produce a product with immediate added value.

C. Cruciblelessness Melting

The ease of free suspension in space has an immediate application to cruciblelessness melting. Generally, benefits can be derived from such melting practice by all materials, including metals and alloys, semiconductor materials, thermoeletric materials, nonmetallic materials (including organics etc.) since during melting the container always interacts with its contents. However, because of anticipated economic considerations, many materials will not assure enough added value through space processing to be practical (steel melting is a good example). The criteria for this study then are processes or processing steps which give added value or uniqueness to materials and expand the technology to allow the final product to be more economically produced, although a penalty is paid for transportation. As an example, a large area of unexplored technology exists in the precision casting of the reactive metals (8), (9) such as Ti, Be, Zr, and the refractory metals, such as Mo, W, Cr, Ta, and Cb. Although these materials can be successfully melted by the skull process, which protects purity by avoiding direct crucible contact, the lack of super-heat restricts casting practice to large, easily fed shapes or pre-shapes suitable for further processing by rolling, extrusion, etc; pouring times are limited to 5 to 7 seconds and section thickness is generally limited to section height (10). Figure III-3 shows schematically various uses for these materials if super heat (and therefore precision casting or die casting) (8), (11) could be made available. It is to be noted that the molding problems associated with these materials is also problematical but compared to container melting to achieve superheat, it is the simpler problem and is amenable to solution (8).

Free suspension processing has side benefits which should not be overlooked; since the molten charge is free of container reactants, its initial purity can be maintained. Also it is obvious that steps to increase purity can be taken, including vacuum melting, zone refining, etc. The availability of sizeable amounts of ultrapure molten metals can increase the use of such materials.

Be is a prime example of a reactive metal which could find many uses because of its high strength, high modulus, and low density if it could be more easily fabricated. Present technology has induced ductility in Be only by single crystal techniques; grain boundary impurities appear to cause severe embrittlement. Space processing, including levitation melting and purification, could conceivably

improve the mechanical properties of Be so that its utility would increase. The electrical characteristics of Be are also interesting if the impurity levels can be reduced. Resistivities at liquid N_2 temperatures of over 500 times less than that of copper at room temperature make Be a prime candidate for cryogenic power cable applications (12). The availability of sizeable amounts of Be can make the requirements of thin-walled tubing or fine wire mesh, cryogenically cooled with liquid N_2 for power transmission systems a reality (13) without resorting to highly refined Cu or Al tubing or mesh operating at liquid H_2 temperatures (14).

It is anticipated that health hazards associated with Be processing would be minimal in space since fume and dust disposal will pose no foreseeable problems. Also, personnel will be already trained to operate in environments in which self-contained life support systems are routine.

D. Avoidance of Crucible Contact During Solidification – Glasses

Many optical devices would benefit from the use of isotropic transparent materials (glasses) with high refractive index. Thin lenses could be made, which would lead to smaller optical instruments. Many glassy systems are known to have high index of refraction but they are usually susceptible to devitrification (recrystallization). Most recrystallization in glassy materials is surface nucleated from contact with crucibles in which melts are made. Levitation melting offers the ability to melt out of contact with crucibles and to explore the possibility of glass forming from compositions which normally would be considered unstable. The possibility also exists that molten materials, which do not normally form amorphous, glassy solids, would do so if they were supercooled and solidified out of contact with crucible materials.

Examples of compositions that are worthy of study in this context are $PbO:SiO_2$ systems rich in PbO (max. RI = 2.6) and $PbO:TeO_2$ systems. Glasses of Ri 2.2 have been obtained from these systems by normal glassforming techniques.

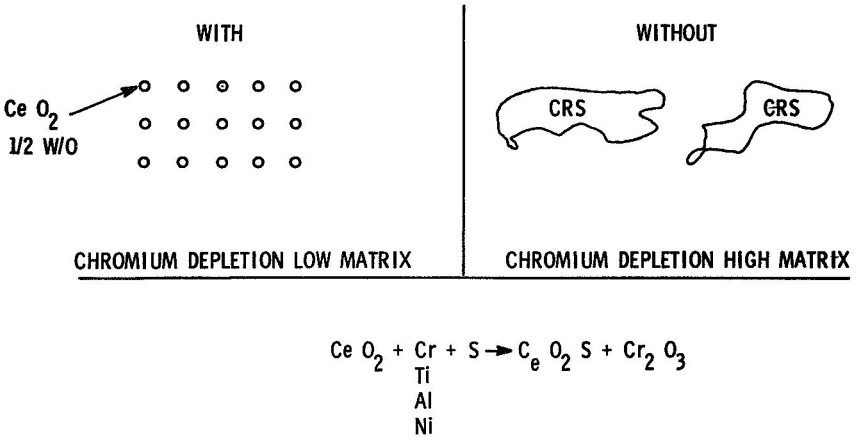

Figure III-1. Rare Earth Oxide Disphersions in Super Alloys

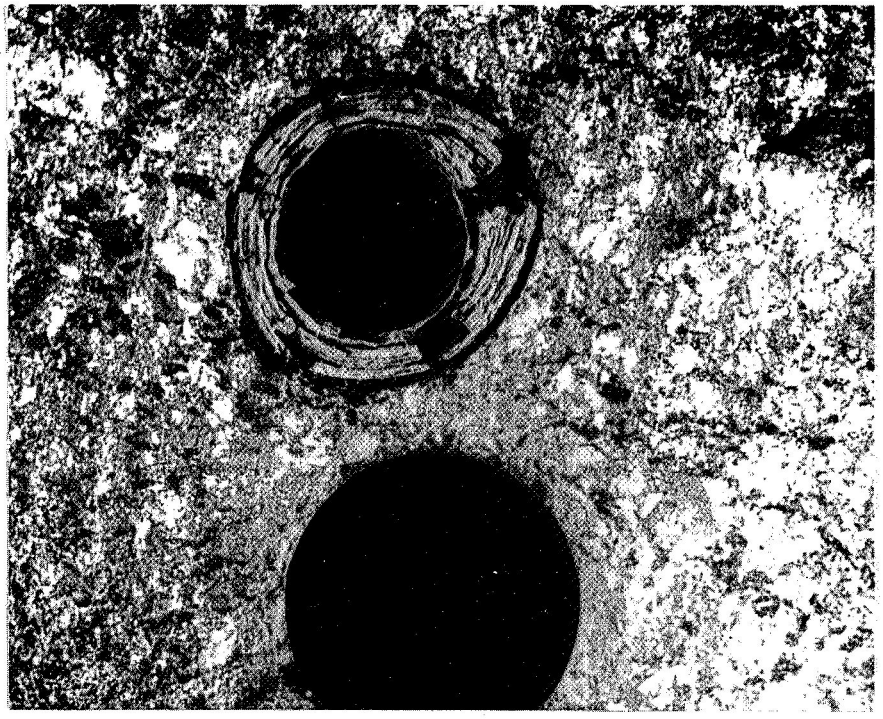

Figure III–2. Comparison of Corrosion Rates with and without Ceruim Oxide Addition

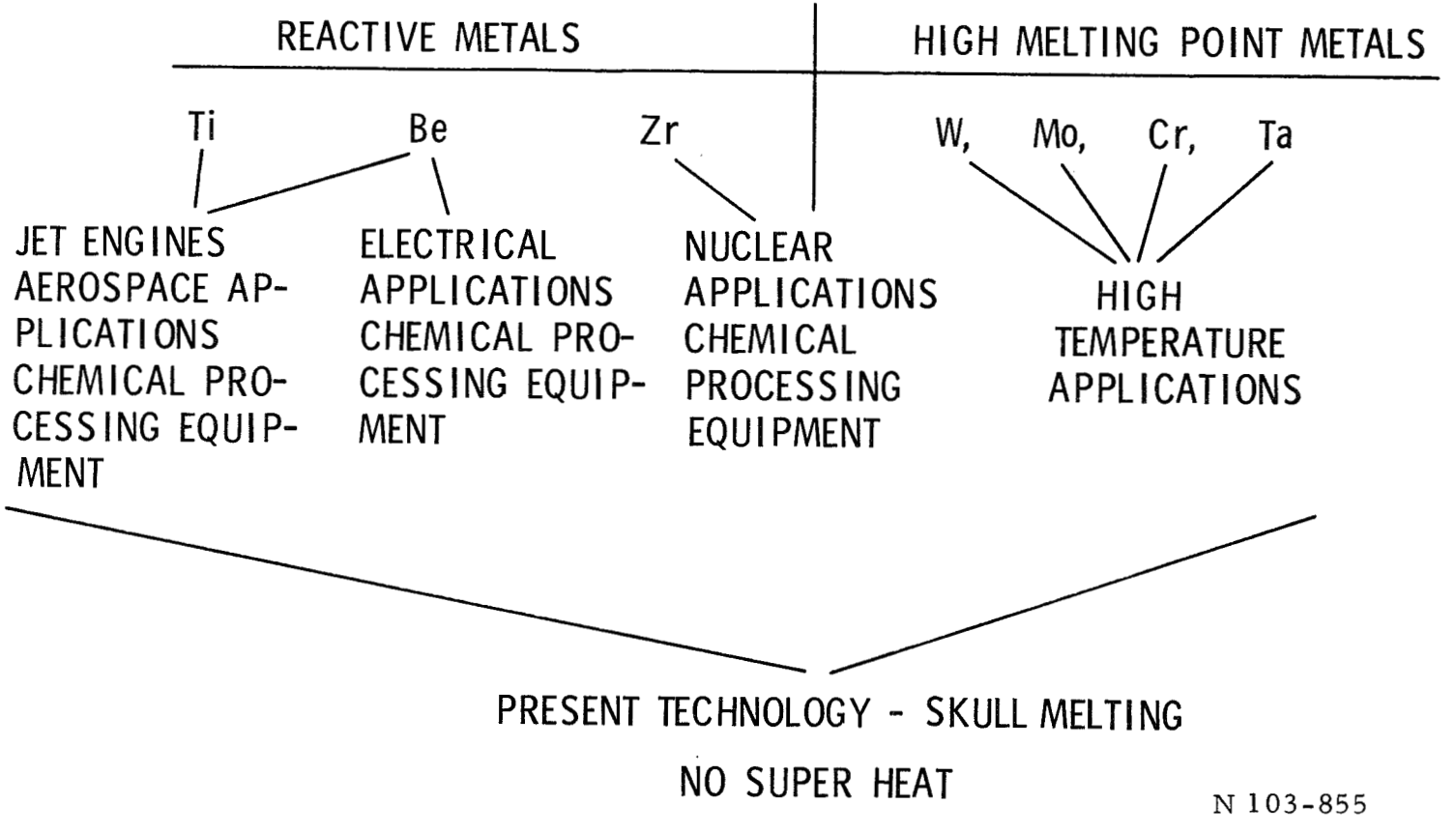

Figure III-3. Crucibleless Melting – Precision Casting, Extrusion Shapes

IV. THEORY OF ELECTROMAGNETIC POSITION CONTROL AND BODY DISTRIBUTED CURRENTS AND FORCES

The theoretical development pursued during the last quarter had as its objectives the examination of a few idealized basic problems which have immediately applicable results to the program and which can be logically extended in the next quarter to obtain solutions to other problems. The objectives of the theoretical development are: (1) to understand the electric currents induced in material bodies of selected composition and state (solid or fluid) when these bodies are immersed in electromagnetic fields; (2) to understand the forces exerted on freely suspended material bodies by electromagnetic fields; and (3) to determine the interaction of material bodies with the electromagnetic field sources through mutual inductance and capacitance so as to describe how the positioning and control devices must function.

A. Vector Potential Induced in Conducting Sphere by Uniform Oscillating Magnetic Field

The first problem considered is that of a conducting sphere in a uniform time harmonic magnetic field. The solution of this problem is applicable to the study of melting conducting materials by induction, fluid currents produced by electromagnetic forces, fluid oscillations due to electromagnetic forces, studies of bubble motion driven by fluid currents, the generation of acoustic waves, and many other topics of interest. This solution is also the first step in understanding positioning forces exerted on the sphere by nonuniform fields, since it can be used to construct a first order solution for force exerted by fields having gradients, as will be shown in following sections.

The problem considered is illustrated in Figure IV-1. Here we have a sphere of uniform conductivity σ immersed in a time harmonic uniform magnetic field $\vec{B}_A = B_o \hat{k} \cos \omega t$, where B_o is the amplitude of the applied field $\vec{B}_A$, $\nu = \omega/2\pi$ is the frequency of the applied field and $\hat{k}_o$ is the unit vector in the z direction. Mathematically the problem can be formulated as the following boundary value problem.

(1) $\nabla^2 \vec{A} = 0$ outside the sphere

(2) $\nabla^2 \vec{A} - \mu\sigma \, \partial \vec{A}/\partial t = 0$ inside the sphere ,

and boundary conditions

As $r \to \infty$, $\vec{A}_e \to \vec{A}_A$

As $r \to o$, $\vec{A}_i$ remains finite

At $r = a$, $\hat{n} \cdot [(\nabla \times \vec{A}_i) - (\nabla \times \vec{A}_e)] = 0$

$$\hat{n} \times [1/\mu_i \nabla \times \vec{A}_i - 1/\mu_o \nabla \times \vec{A}_e] = 0 \ .$$

Here $\vec{A}$ is the vector potential and the magnetic induction $\vec{B}$ is just $\nabla \times \vec{A}$.

Thus $\vec{B}_A = \nabla \times \vec{A}_A$ is the applied magnetic field

$\vec{B}_e = \nabla \times \vec{A}_e$ is the total external magnetic field

$\vec{B}_i = \nabla \times \vec{A}_i$ is the magnetic field within the sphere, and solving the boundary value posed above for $\vec{A}_e$ and $\vec{A}_i$ gives $\vec{B}_e$ and $\vec{B}_i$.

The above problem has been treated by Smythe (15) and others. We have extended the treatment of Symthe to include the field inside the sphere, the instantaneous forces acting at all points on and within the sphere, and the time averaged forces acting at all points on and within the sphere. Rather than present the detailed solution to this problem which can be found in the above reference we shall outline the solution and discuss the results and our extension in detail.

To simplify the mathematical solution of the problem it is convenient to replace $\vec{B}_A = B_o \cos \omega t \hat{k}$ by $B_A = B_o e^{j\omega t}\hat{k}$, where $e^{j\omega t} = \cos \omega t + j \sin \omega t$, where $j = \sqrt{-1}$.

We can then write equation 2 as

$$\nabla^2 \vec{A} - j \omega \mu \sigma \vec{A} = 0.$$

We must remember that in the solutions we must multiply by $e^{j\omega t}$ and take the real part as the actual solution.

The vector potential $\vec{A}_A$ of $\vec{B}_A$ can be written in spherical polar coordinates as $\vec{A}_A = \frac{1}{2} B_o r \sin \theta \hat{\Phi}$, where $\hat{\Phi}$ is the unit vector in the Φ direction (see Figure IV-2). Since the exciting vector potential has only a Φ component, we expect the currents induced in the sphere to have only a Φ component and hence the vector potential $\vec{A}_i$, to have only a Φ component. Since the total external vector potential is due to the applied field and the induced currents, we then have the vector potential external to the sphere; $\vec{A}_e$ must also have only a Φ component. The results obtained by Smythe (15) after writing $\nabla^2 \vec{A} = 0$ and $\nabla^2 \vec{A} - j \omega\mu\sigma \vec{A} = 0$ in spherical polar coordinates and solving the boundary value problem by separation of variables is

$$\vec{A}_e = [\tfrac{1}{2} B_o r \sin \theta + D B_o \sin \theta / r^2] \hat{\Phi}$$

$$\vec{A}_i = \tfrac{1}{2} B_o C r^{-1/2} I_{3/2} \{ (jP)^{1/2} r \} \sin \theta \hat{\Phi},$$

where

$$D = \frac{(2\mu + \mu_o)\, v\, I_{-1/2}\{v\} - \left[\mu_o (1 + v^2) + 2\mu\right] I_{1/2}\{v\}}{(\mu - \mu_o)\, v\, I_{-1/2}\{v\} + \left[\mu_o (1 + v^2) - \mu\right] I_{1/2}\{v\}} \quad a^3$$

and

$$C = \frac{3\mu\, v\, a^{3/2}}{(\mu - \mu_o)\, v\, I_{-1/2}\{v\} + \left[\mu_o (1 + v^2) - \mu\right] I_{1/2}\{v\}}$$

Here we have I_n as the symbol for the Bessel function of order n, $P = \sigma\mu\omega$ and $v = (jP)^{1/2}\, a$. The skin depth δ is a basic parameter of the solution and

$$\delta = \sqrt{\frac{2}{\sigma\, \mu\, \omega}} = \sqrt{\frac{2}{P}}$$

If we consider the conducting sphere as not permeable so that $\mu = \mu_o$, then C further simplifies to be

$$C = \frac{3\, a^{3/2}}{v\, I_{1/2}\{v\}}$$

B. Electric Current Density Within the Sphere

The current density is given by $\vec{J} = \sigma \vec{E}$ within a conductor and

$$\vec{E} = -\frac{\partial \vec{A}_i}{\partial t} = -j\, \omega \vec{A}_i \quad ,$$

so

$$\vec{J}_i = -j\, \omega\, \sigma\, \vec{A}_i = -j\, P\, \mu^{-1}\, \vec{A}_i \quad .$$

We can write the Bessel functions in terms of hyperbolic functions as

$$I_{1/2}\{v\} = \left(\frac{2}{\pi v}\right)^{1/2} \sinh v$$

and

$$I_{3/2}\{v'\} = \left(\frac{2}{\pi v'}\right)^{1/2} \left[\cosh v' - \frac{1}{v'} \sinh v'\right]$$

where we let $v' = (jP)^{1/2} r$. Using these expressions and writing out $\vec{J_i} = -j P\mu^{-1} \vec{A_i}$, we obtain finally

$$\vec{J_i} = \frac{3 a B_o \sin\theta}{\sqrt{2}\, \delta \mu (\alpha^2 + \beta^2)} \left[\frac{Y - jX}{r} \right] \hat{\Phi} ,$$

where X and Y are real functions of r, a and δ.

Then $\vec{J_i} = J_i e^{j\omega t} \hat{\Phi}$ is the complete time harmonic current density and the actual current density is $R_e \; J_i e^{j\omega t} \hat{\Phi}$. Let us write J_i as S + j T and $e^{j\omega t}$ as cos ωt + j sin ωt, so

$$J_i e^{j\omega t} = (S + j\, T)(\cos \omega t + \sin \omega t)$$

$$= (S \cos \omega t - T \sin \omega t) + j (T \cos \omega t + S \sin \omega t) .$$

Then

$$J_i = R_e \left\{ J_i e^{j\omega t} \right\} = \sqrt{S^2 + T^2} \cos \left[\omega t + \tan^{-1} (T/S) \right] .$$

When

$$t = 0, \quad J_i = \sqrt{S^2 + T^2} \cos \left[\tan^{-1} (T/S) \right] = S$$

finally we have

$$\vec{J_i} = \frac{3 a B_o \sin\theta}{\sqrt{2}\, \delta \mu (\alpha^2 + \beta^2) r} \sqrt{Y^2 + X^2} \cos \left[\omega t + \tan^{-1} \left\{ \frac{-X}{Y} \right\} \right] \hat{\Phi},$$

and at t = 0

$$\vec{J_i} = \frac{3 a B_o \sin\theta}{\sqrt{2}\, \delta \mu (\alpha^2 + \beta^2)} \frac{Y}{r} \hat{\Phi} .$$

The ratio a/δ is the main parameter, where a = the radius of the sphere and $\delta = \sqrt{2/\sigma\mu\omega}$ is the skin depth and is a function of the material properties σ = conductivity, μ = permeability, and the time harmonic frequency of the applied magnetic field $\nu = \omega/2\pi$. The parameters a and δ will be shown to play a large role in the selection of materials and exciting frequencies in all phases of material manipulation.

The results of analysis lead to the following conclusions.

(1) At low frequencies where $a/\delta << 1$ and of course, since $0 \leq r \leq a$, $r/\delta << 1$

(a) The lines of current are circles centered on the z axis.

(b) The dominant term of the current density is proportional to r sin θ and is 90^{o} out of phase with the incident magnetic field.

(2) At high frequencies where $a/\delta >> 1$

(a) The induced current may be through of as flowing in a layer whose thickness is of the order of δ and the amplitude of the current density decreases exponentially in the direction of the normal.

(b) The current is approximately in phase with the incident field. Its direction is such that the resulting magnetic field is opposite in direction to the incident field.

Figure IV-3 shows the positive half cycle average of $\vec{J}$ for $\theta = 90^{o}$ as a function of radial distance from the center of a 0.4125 in. radius aluminum sphere for values of a/δ ranging from 0.5 to 13.

C. Magnetic Field Induced Within the Sphere

For computation of distributed body forces, it is necessary to obtain the magnetic field within the sphere. This is given by $\nabla \times \vec{A}_i$ and in spherical coordinates

$$\nabla \times \vec{A}_i = \frac{1}{r^2 \sin\theta} \begin{vmatrix} \hat{r} & r\hat{\theta} & r \sin\theta \hat{\Phi} \\ \partial/\partial r & \partial/\partial\theta & \partial/\partial\Phi \\ A_r & rA_\theta & rA_\Phi \sin\theta \end{vmatrix}$$

Since $\vec{A_i} = A_i \hat{\Phi}$ and $A_r = A_\theta = 0$ we have

$$B_i = \nabla \times \vec{A_i} = \frac{1}{r \sin\theta} \frac{\partial (A_i \sin\theta)}{\partial \theta} \hat{r} - \frac{1}{r} \frac{\partial (r A_i)}{\partial r} \hat{\theta} ,$$

So

$$B_i = \frac{1}{r \sin\theta} \frac{\partial}{\partial \theta} (\sin\theta A_i)$$

$$B_{i\theta} = - \frac{1}{r} \frac{\partial (r A_i)}{\partial r}$$

and

$$B_{i\Phi} = 0 .$$

The actual expressions obtained are

$$B_{ir} = \left(\frac{3a \delta B_o}{\sqrt{2}\, r^2}\right)\left(\frac{1}{\alpha^2 + \beta^2}\right) (X + jY) \cos\theta$$

$$B_{i\theta} = - 1/2\, B_o C \sin\theta \left\{ \left(\frac{\sqrt{2}\delta}{\pi r}\right)^{1/2} \left[N(r) + j Q(r) \right] \right.$$

$$\left. + 1/2 \left(\frac{\sqrt{2}\,\delta}{\pi r}\right)^{1/2} \frac{1}{r^2} \left[G(r) + j H(r) \right] \right\} ,$$

where N, Q, G and H are complicated functions of r, a and δ obtained by differentiating X and Y.

Remembering that we must multiply by $e^{j\omega t}$ and take the real part, we have

$$B_{ir} = R e \left\{ B_{ir} e^{j\omega t} \right\}$$

$$B_{i\theta} = R e \left\{ B_{i\theta} e^{j\omega t} \right\} .$$

Figures IV-4 and IV-4A are plots of the radial magnetic field at $\theta = 45^{o}$ as a function of radial distance for an aluminum sphere having a radius a = 0.415 in. for values of a/δ from 0.1 to 13. Figures IV-5 and IV-5A are plots of the θ component of the field at $\theta = 45^{o}$ as a function of radial distance for values of a/δ from 0.1 to 13.

From these figures we can see that as a/δ increases the field penetrates the sphere to a lesser and lesser extent. For $a/\delta >> 1$ the field is almost entirely excluded from the sphere.

D. Body Distributed Lorentz Forces Within Suspended Sphere

1. Instantaneous Forces Acting On and Within the Sphere

The instantaneous forces acting at any point on and within the sphere are proportional to $Re\,(\vec{J}) \times Re\,(\vec{B})$. We have then that

$$\vec{F}_{ir} \propto - J_i B_{i\theta}\,\hat{r}$$

$$\vec{F}_{i\theta} \propto J_i B_{ir}\,\hat{\theta}\ .$$

Figures IV-6 and IV-7 are plots of $J_i B_{i\theta}$ and $J_i B_{ir}$ for $\theta = 45^{o}$ for an aluminum sphere of radius 0.4125 in. for values of a/δ from 1 to 10. It can be seen that as a/δ increases more and more force is exerted on the outer layers of the sphere.

2. Time Averaged Forces Acting On and Within the Sphere

If we write

$$\vec{J} = J_i\, e^{j(\omega t + \psi_1)}\hat{\Phi}$$

$$\vec{B}_{ir} = B_{ir}\, e^{j(\omega t + \psi_2)}\hat{r}$$

$$\vec{B}_{i\theta} = B_{i\theta}\, e^{j(\omega t + \psi_3)}\hat{\theta}\ ,$$

where the actual magnetic field values and current density are the real parts of these terms the time average of $R_e\,(\vec{J}) \times R_e\,(\vec{B})$ is $< R_e\,(J) \times R_e\,(B) > \propto < F_{ir} > \hat{r} + < F_{i\theta} > \hat{\theta}$, and on expanding this one arrives at

$$< F_{ir} > \propto -\tfrac{1}{2}\,|J_i B_{i\theta}|\cos(\psi_1 - \psi_3)$$

$$< F_{i\theta} > \propto \tfrac{1}{2}\,|J_i B_{ir}|\cos(\psi_1 - \psi_2)\ ,$$

where here J_i, B_{ir}, $B_{i\theta}$ are the phasor quantities written above.

It is found that for a uniform field $< F_{i\theta} > = 0$ and the forces exerted on the sphere by the field are all magnetostrictive. Figure IV-8 is a plot of the radial component of $< R_e (\vec{J}) \times R_e (\vec{B}) >$ for θ from 0 to 90^o vs. radial distance for an aluminum sphere of radius a = 0.4125 in. and $a/\delta = 5$. Thus from a uniform field no positioning forces are obtained but magnetostrictive forces which excite fluid currents and oscillations are obtained.

E. Positioning Forces Exerted on a Conducting Sphere by a Coil

The basic problem is that a conducting sphere in the time harmonic field of a coil. This is shown in Figure IV-9. Fromm and Jehn (16), Okress (17) and others have obtained an approximate formula for computing the force exerted on the sphere by the coil, which has proved useful for rough, approximate computations. It is a good relation to start with as it gives a reasonably good estimate of the magnitudes of the forces considered.

Grant and West (18) have obtained a solution for the problem of a conducting sphere in a dipole field. When the coil is far from the sphere it is essentially a dipole so that this problem is relevant to the problem at hand and forms a basis for the approximate formula of Fromm and Jehn. Here we want to consider the qualitative results of the solution. It is pointed out in (18) that "if the dipole is far from the sphere, the solution degenerates to that for a uniform field." Then the "secondary field of the sphere will be identical with the field of a simple magnetic dipole." This is the basis of the approximate formula of Fromm and Jehn.

The approach of Fromm and Jehn is to consider the sphere as having a magnetic moment equivalent to that which it would have if placed in a time harmonic uniform field. From Section II we see that the external vector potential $\vec{A}_e$ is just

$$\vec{A}_e = \hat{\Phi} \tfrac{1}{2} B_o (r + D/r^2) \sin\theta \ ,$$

so that the contribution from the sphere is

$$\vec{A}_s = \hat{\Phi} \tfrac{1}{2} B_o D \sin\theta / r^2 \ .$$

For a nonpermeable conducting sphere where $\mu = \mu_o$

$$D = \frac{3 v I_{-1/2}\{v\} - (3 + v^2) I_{1/2}\{v\}}{v^2 \ I_{1/2}\{v\}} \ ,$$

where v and I have been discussed in Section II.

The vector potential $\vec{A}_s$ can be approximated by a current in a circular loop of radius a (that of the sphere) and current I_2 which is just

$$\vec{A}_\ell = (\tfrac{1}{4} a^2 \mu_o I_2) \sin\theta / r^2 \hat{\Phi} .$$

Equating $\vec{A}_s$ to $\vec{A}_\ell$ we obtain

$$\tfrac{1}{4} a^2 I_2 = \tfrac{1}{2} H_o D ,$$

or

$$\pi a^2 I_2 = 2\pi H_o D ,$$

so that the magnetic moment of the sphere ($2\pi H_o D$) is equal to the dipole moment of this equivalent loop. The equivalent loop current I_2 is just

$$I_2 = 2 H_o D/a^2 .$$

By considering the force exerted between the equivalent loop and a single current loop, an expression for the force is obtained:

$$F_z = (3/50) \pi^2 I_1^2 G(x) A(y) (R_2/R_1)^3 ,$$

where $x = R_2/\delta$

$y = z/R_1$

and R_2 = a, the radius of the sphere

R_1 = the radius of the loop.

Here

$$G(x) = - R_e \{ D \} /a^3 ,$$

where $R_e \{ D \}$ is the real part of D and

$$A(y) = y/(1 + y^2)^4 .$$

For a coil of more than 1 turn the expression for A (y) becomes more complicated; and if $(z - z_n)$ is the distance from the nth loop to the sphere and b_n, the radius of the nth turn, we replace A (y) by A $[b_n, (z - z_n)]$ which will involve a sum over the n turns. The expression for the F_2 is

$$F_z = \frac{3}{2} \pi \mu_o I_1^2 a^3 G(x) \sum_n \frac{b_n^2}{\left[b_n^2 + (z - z_n)^2\right]^{3/2}} \sum_n \frac{b_n^2 (z - z_n)}{\left[b_n^2 + (z - z_n)^2\right]^{5/2}}$$

and still has the form of that of a single loop.

Using the expression for a single loop and approximating the coil used by a loop of current (NI) we made comparisons between the measured force on aluminum and copper spheres having respective radii $R_2 = 0.4125$ in. and 0.6075 in. The equation is good to within a factor of 2 over the entire range of distances from 0 out to greater than 3 coil radii. Figures IV-10, 10A, 11, and 11A are computations of

$$\frac{F_z}{\frac{4}{3} \pi R_2^3 \rho I_1^2}$$

where ρ is the density. This is the acceleration imparted to the sphere as a function of distance from the coil per unit current^2 for values of a/δ $(a = R_2)$ ranging from 0.1 to ≥ 10. As has been stated where experimental measurements were made the agreement was good considering the crude approximations. In fact Fromm and Jehn report that the formula holds reasonably well for $R_2/R_1 \approx$ ½ and at all distances from the coil.

It can be concluded that for rough engineering calculations this approximate solution is useful. For computations of fluid motion, however, a more exact treatment is necessary and will be performed.

F. Dielectric Positioning

During this quarter the theoretical work on dielectric spheres in electromagnetic fields has not been advanced to the level where we have studied conducting spheres. This work is in preparation and will be reported. An order of magnitude calculation has been made for the magnitude of the electric fields necessary to exert a few dynes of force on a Pyrex glass sphere of radius $a = 0.4125$ in. Consider a dielectric sphere in a time harmonic electric field. To the first order an induced polarization

$$\vec{P} = 4\pi \epsilon_o a^3 |\vec{E}| \left[\frac{\varkappa_e - 1}{\varkappa_e + 2}\right] \hat{k}$$

will be induced in the sphere by a field E cos $\omega t \hat{k}$;

Here $\vec{P}$ is the induced polarization

ϵ_o is the permittivity of free space

κ_e is the relative permittivity of the dielectric.

To the first order the force acting on the dielectric sphere is $\vec{F} = (\vec{P} \cdot \nabla)\vec{E}$, and this is

$$\vec{F} = 4\pi \epsilon_o R_2^3 \left[\frac{\kappa_e - 1}{\kappa_e + 2}\right] E \frac{\partial E}{\partial z} \hat{k}$$

We shall take a field whose gradient is given by $dE/dz = E/3$ (volts/cm/cm) or $E/3 \times 10^2$ volts/meter^2,

so that

$$F_z = 4\pi \epsilon_o \left[\frac{\kappa_e - 1}{\kappa_e + 2}\right] R_2^3 \frac{E^2}{3} \times 10^2 .$$

Using $R_2 = 0.4125$ in. $= 0.0104775$ meters

$\kappa_e = 5.1$ for Pyrex glass

$\epsilon_o = 8.854 \times 10^{-12}$ farads/meter,

we have

$$F = 2.46\, E^2 \times 10^{-10} \text{ dynes}.$$

Therefore, to get a force of 2.46 dynes with a field having the above gradient we would need $E = 10^5$ volts/meter or 10^3 volts/cm.

This result shows that dielectric positioning of a small pyrex glass sphere requires fields of the order of 10^3 volts/cm to get a few dynes of force. For positioning in the weightless state this is not an unreasonable field to generate. More exact calculations will be presented in the next quarterly report for selected electric field shapes.

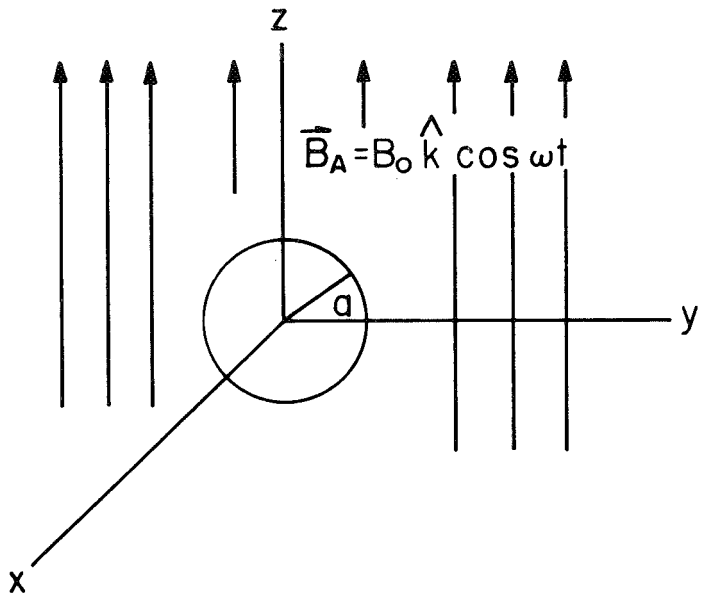

Figure IV-1. Conducting Sphere in a Uniform, Time Harmonic Magnetic Field

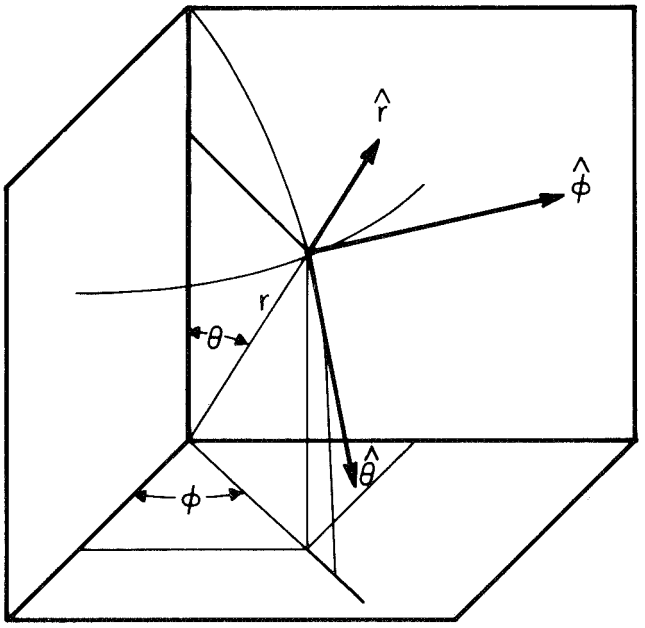

Figure IV-2. Spherical Coordinate System

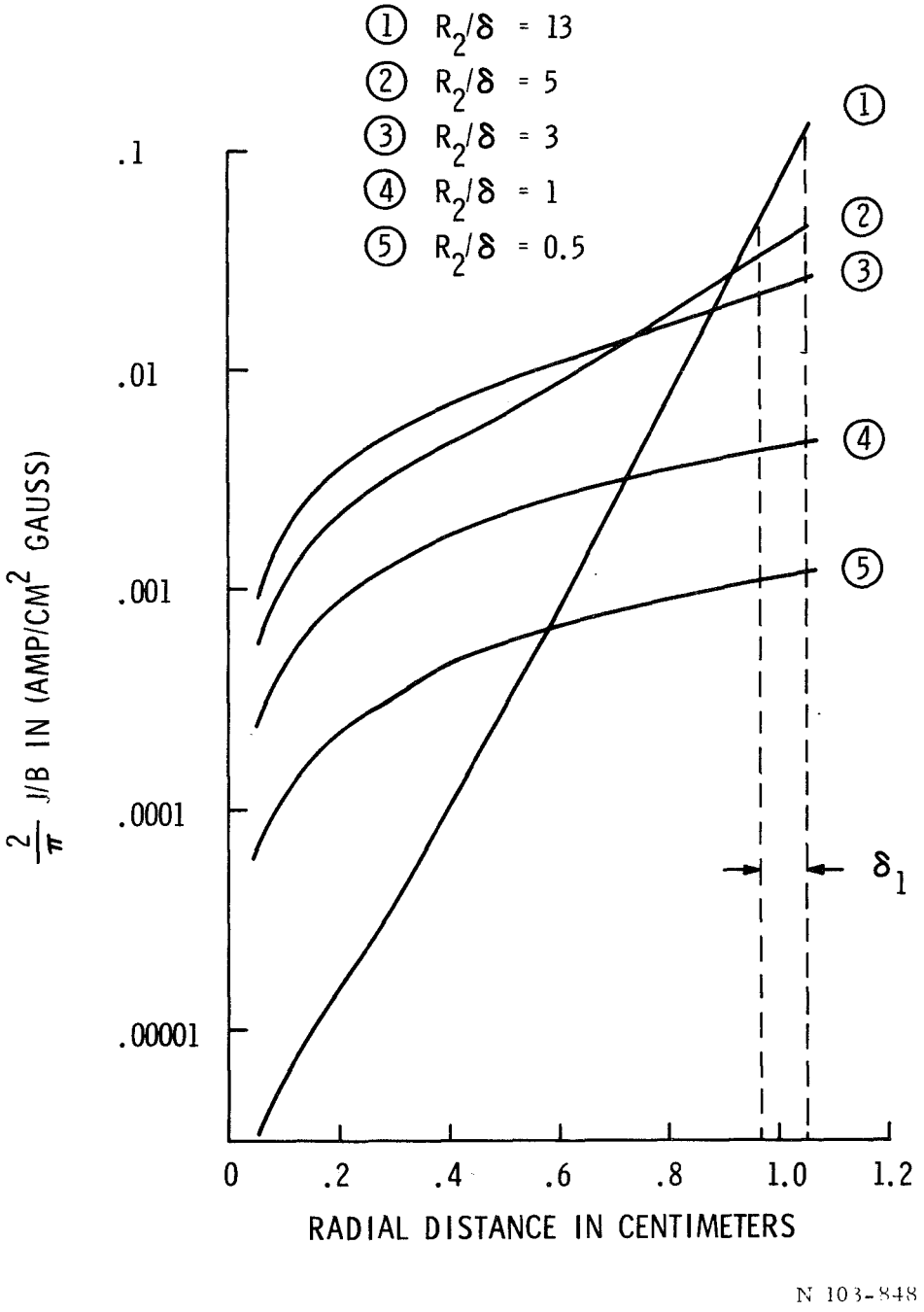

Figure IV-3. Positive Cycle Average of Current Density per Unit Magnetic Induction vs. Radial Distance From Center of Aluminum Sphere 0.4125 Radius for $\theta = 90^o$

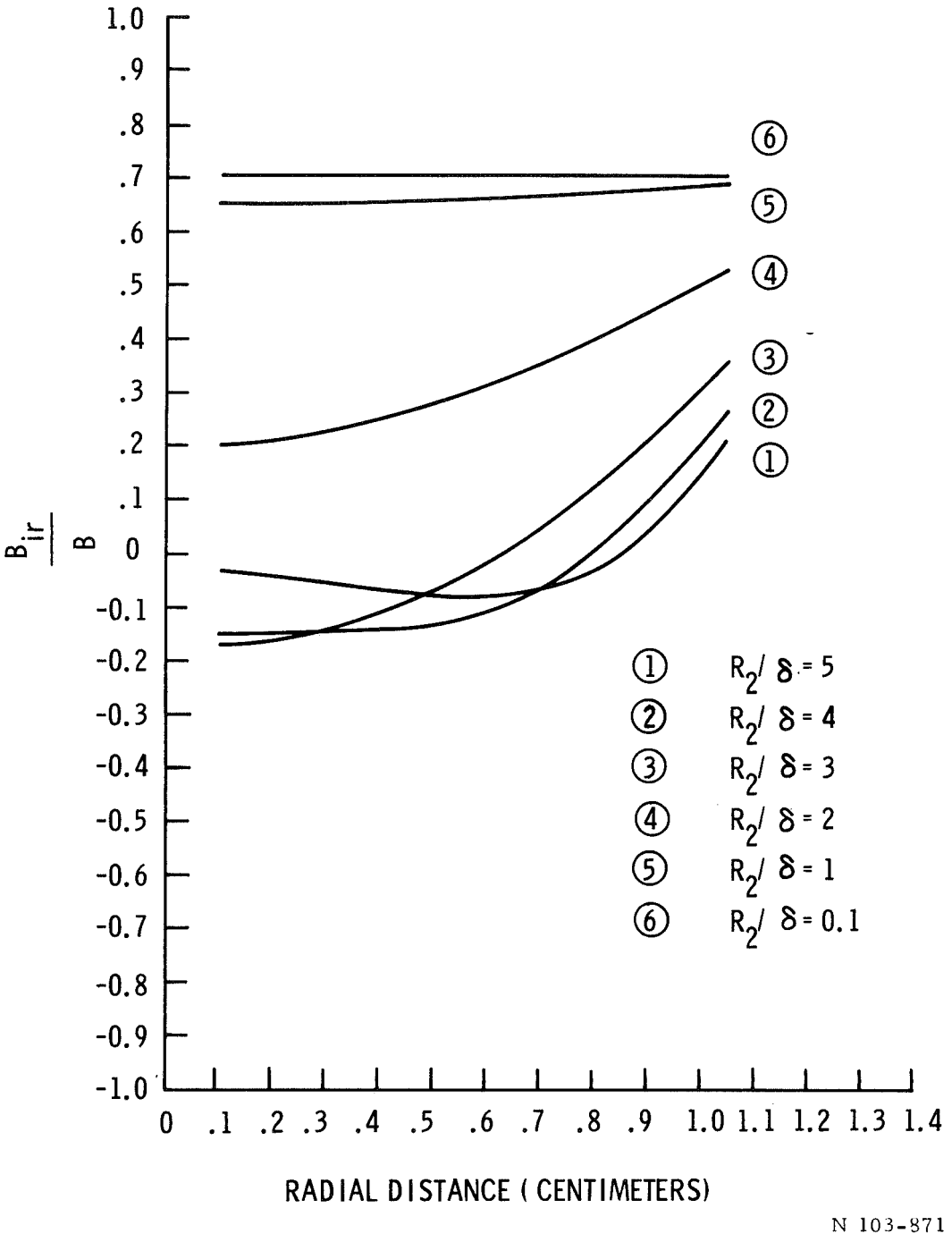

Figure IV-4. Radial Component of Magnetic Field per Unit Magnetic Induction in Aluminum Sphere of Radius $R_2 = .4125$ Inches at Colatitude $\theta = 45^o$ Showing Penetration of Field into Sphere as a Function of Skin Depth

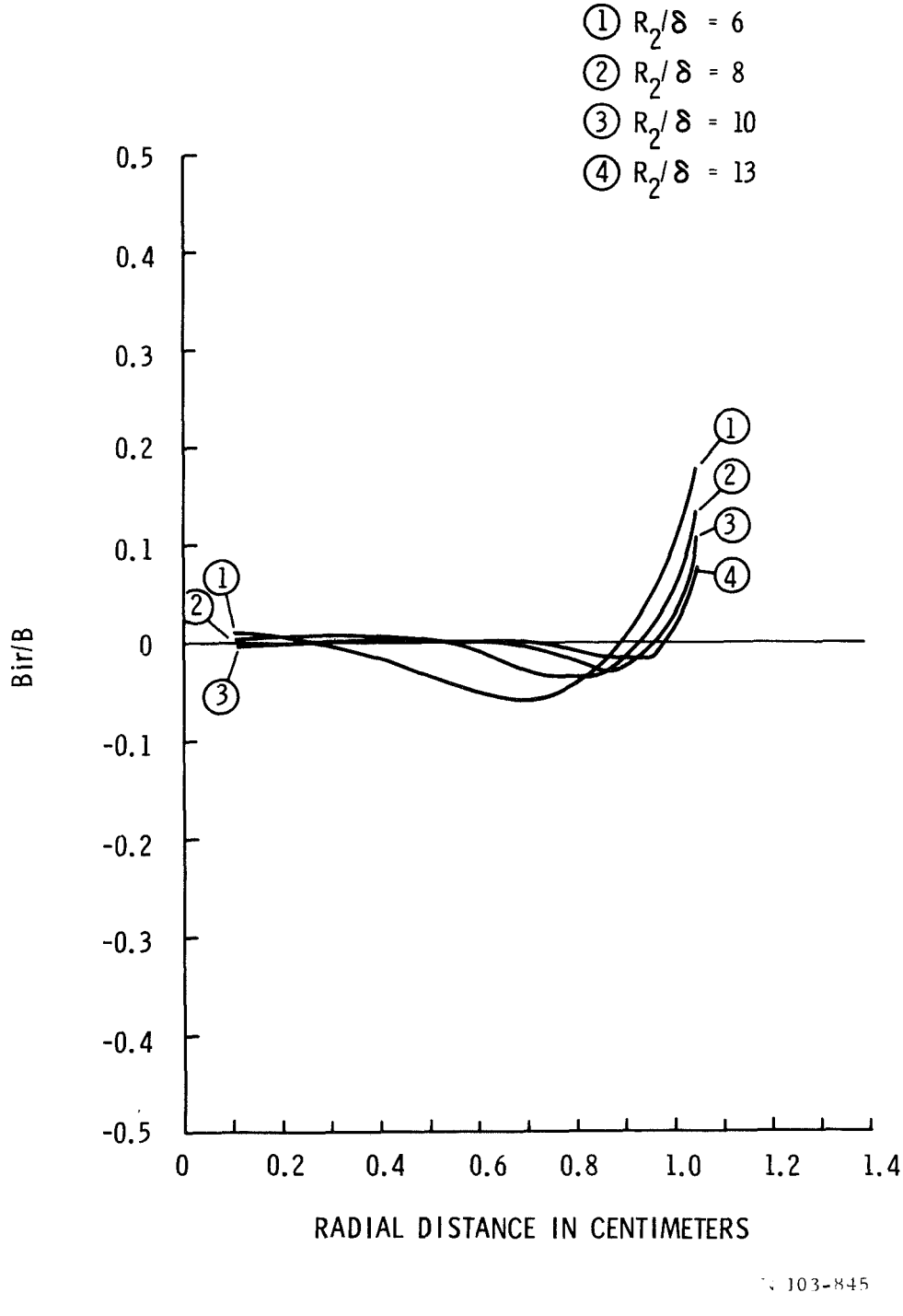

Figure IV-4A. Radial Component of Magnetic Field per Unit Magnetic Induction in Aluminum Sphere of Radius R_2 = .4125 Inches at Colatitude $\theta = 45^o$ Showing Penetration of Field into Sphere as a Function of Skin Depth

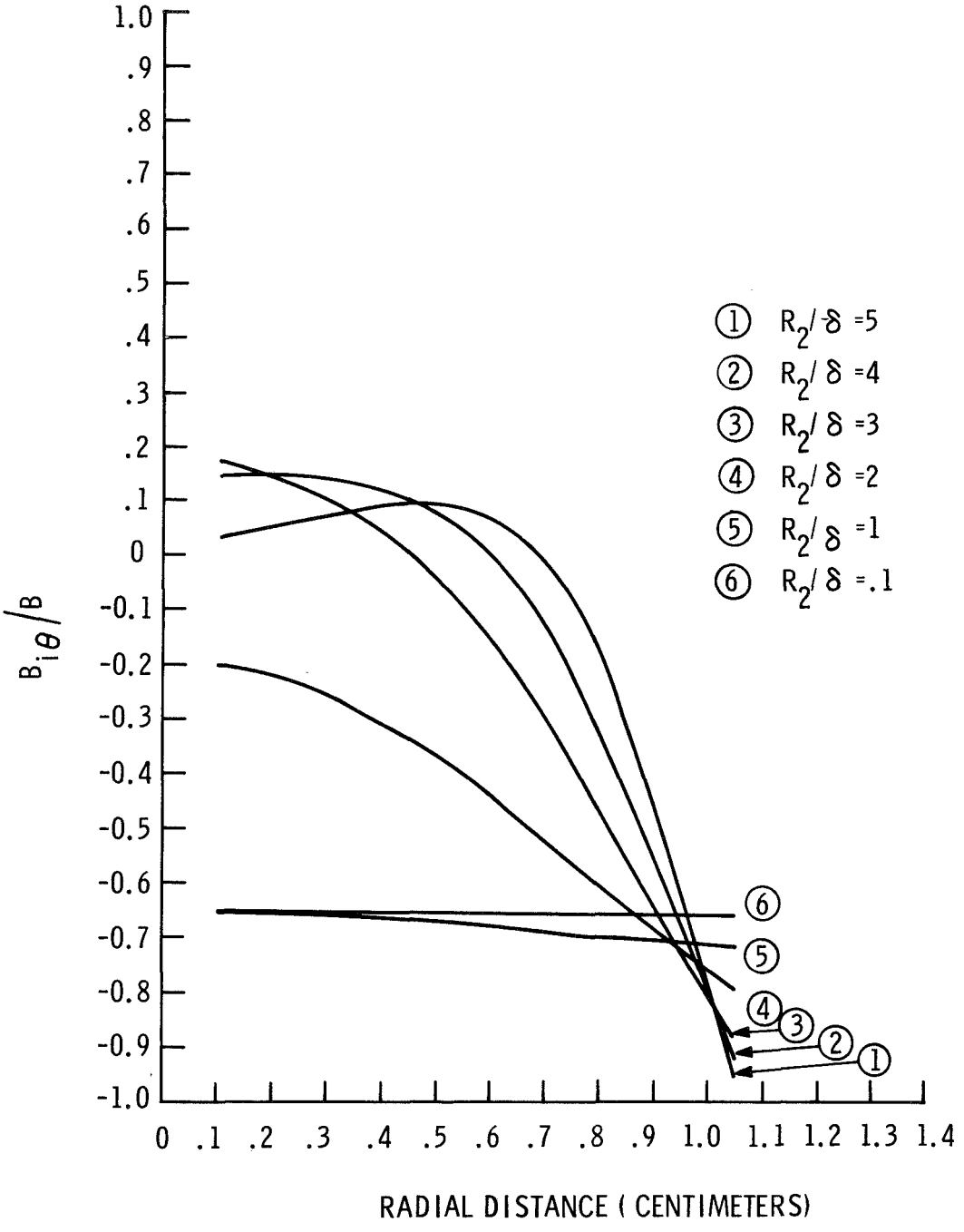

Figure IV-5. θ Component of Magnetic Field per Unit Magnetic Induction in Aluminum Sphere of Radius R_2 = 0.4125 Inches at Colatitude θ = 45° Showing Penetration of Field into Sphere as a Function of Skin Depth

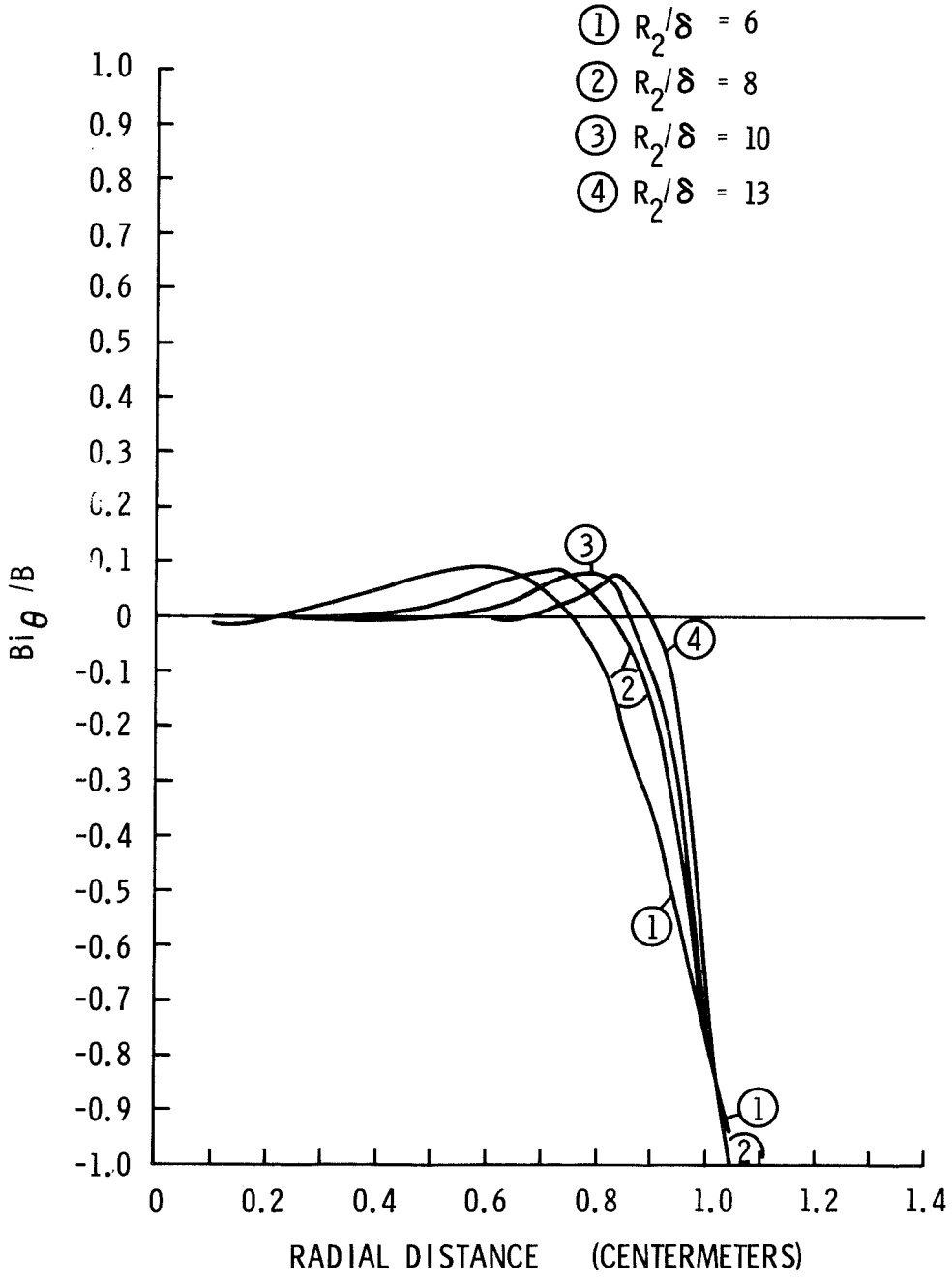

Figure IV-5A. θ Component of Magnetic Field per Unit Magnetic Induction in Aluminum Sphere of Radius R_2 = 0.4125 Inches at Colatitude θ = 45° Showing Penetration of Field into Sphere as a Function of Skin Depth

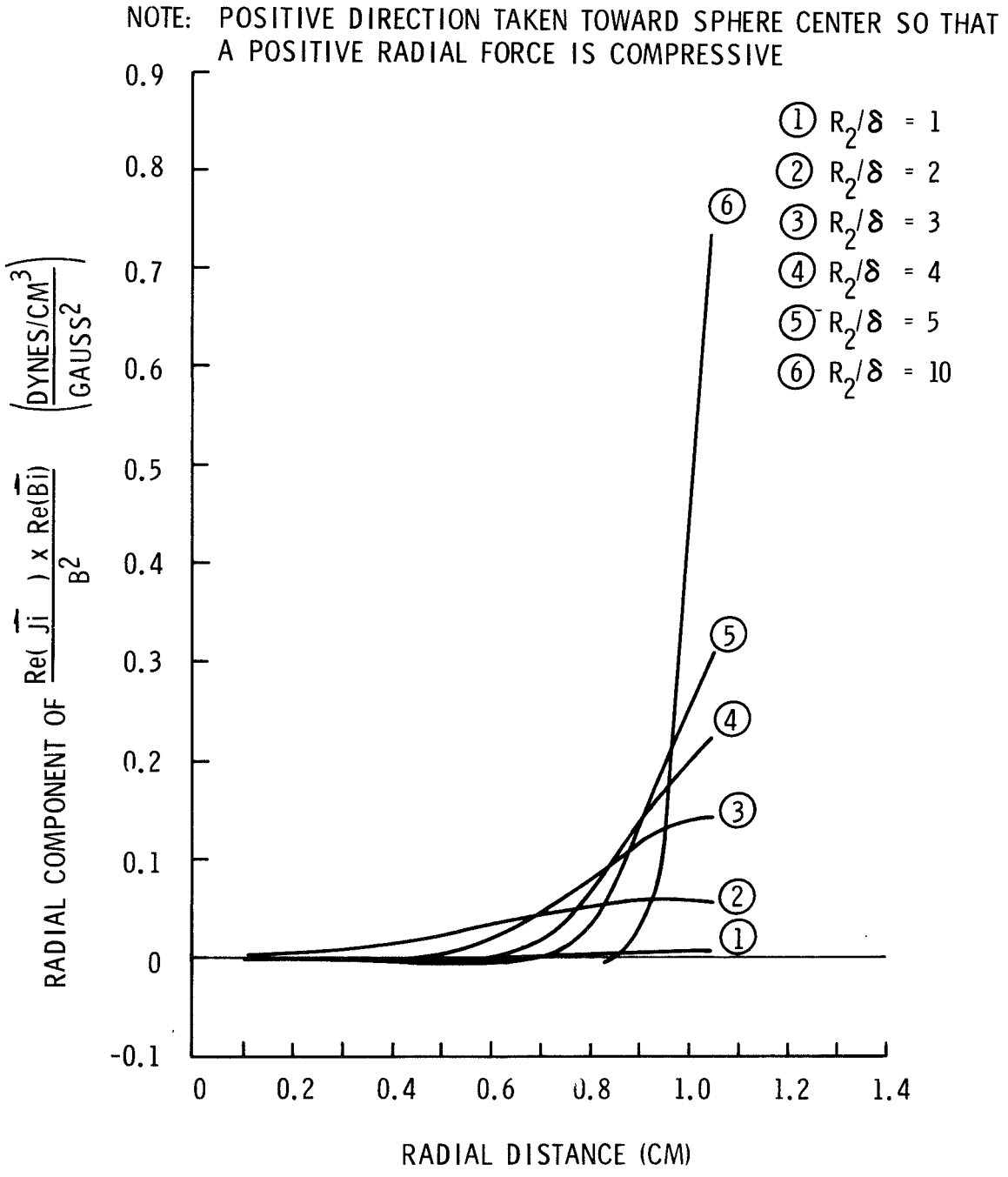

Figure IV-6. Radial Component Force/Volume per Unit Magnetic Induction Squared for Aluminum Sphere R_2 = .4125 Inches at $\theta = 45^o$ as a Function of Skin Depth

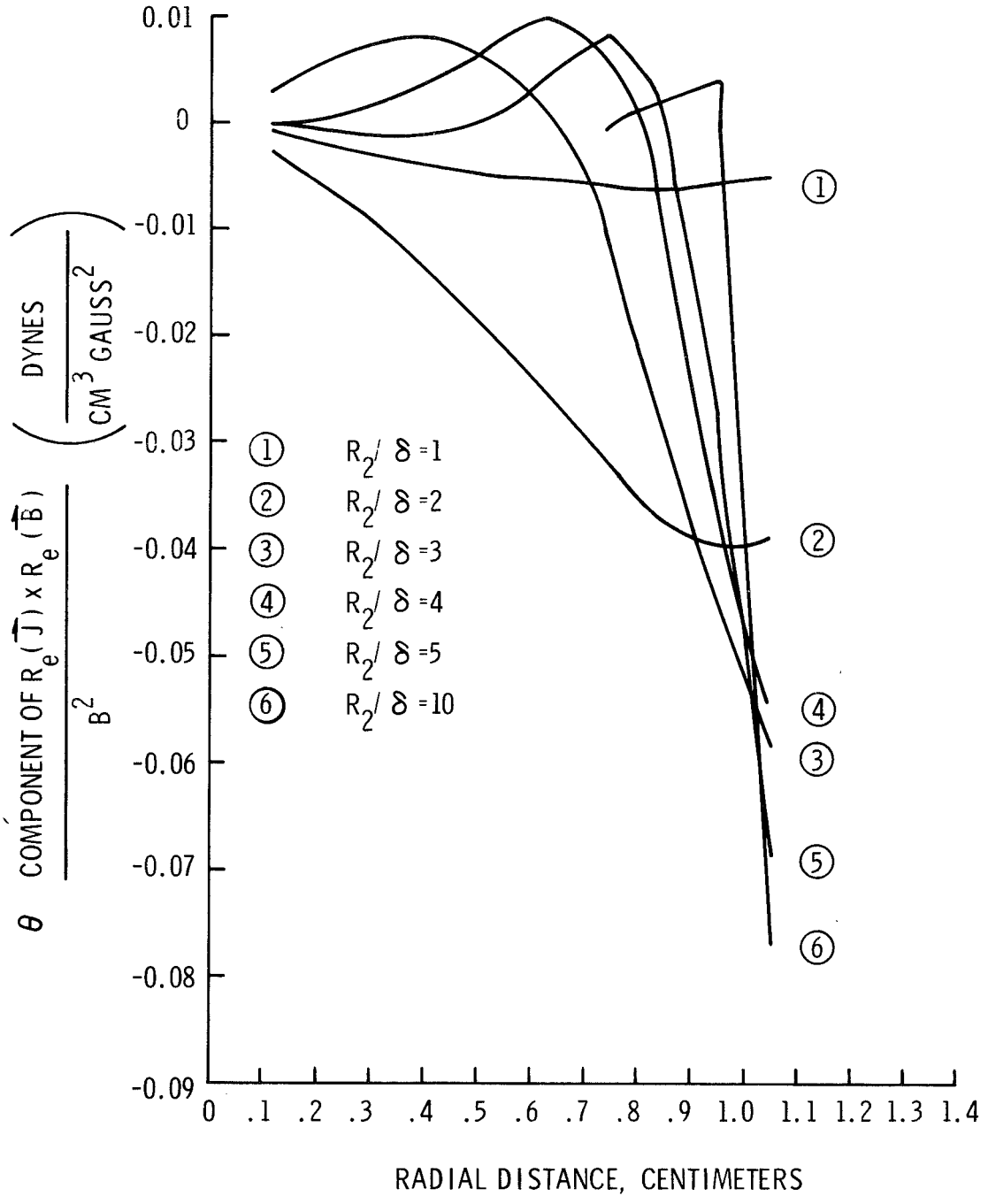

Figure IV-7. θ Component Force/Volume per Unit Magnetic Induction Squared for Aluminum Sphere R_2 = 0.4125 Inches at θ = 45° as a Function of Skin Depth

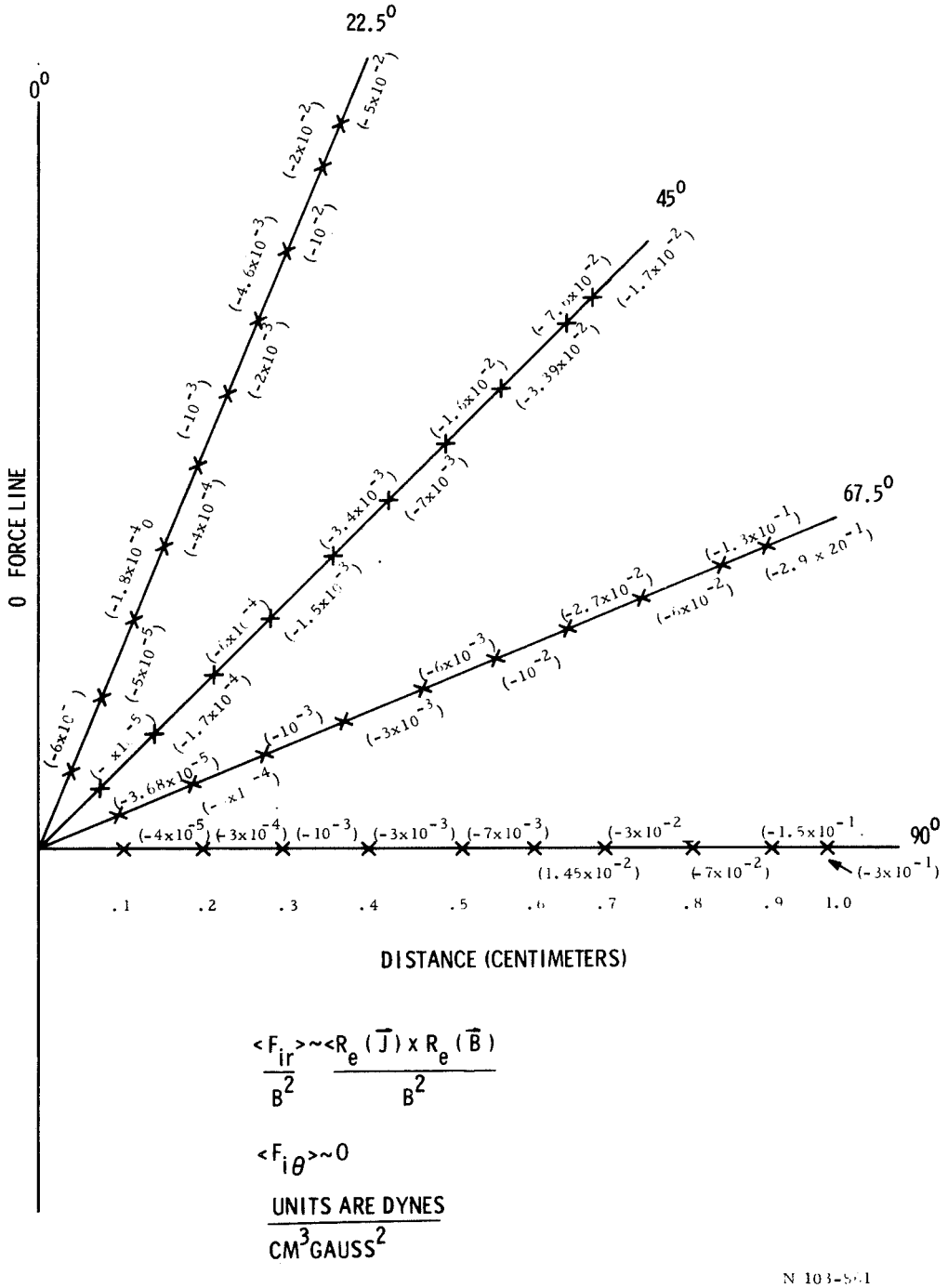

Figure IV-8. Time Average Radial Force per Unit Magnetic Induction Squared in Units of Dynes/cm^3 gauss^2

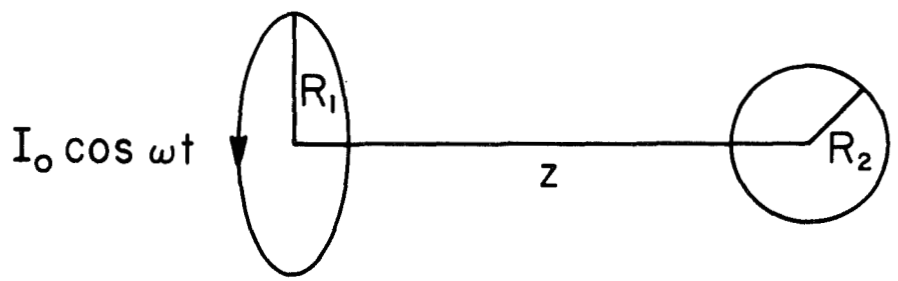

N 103-863

Figure IV-9. Conducting Sphere in the Time Harmonic Field of a Coil

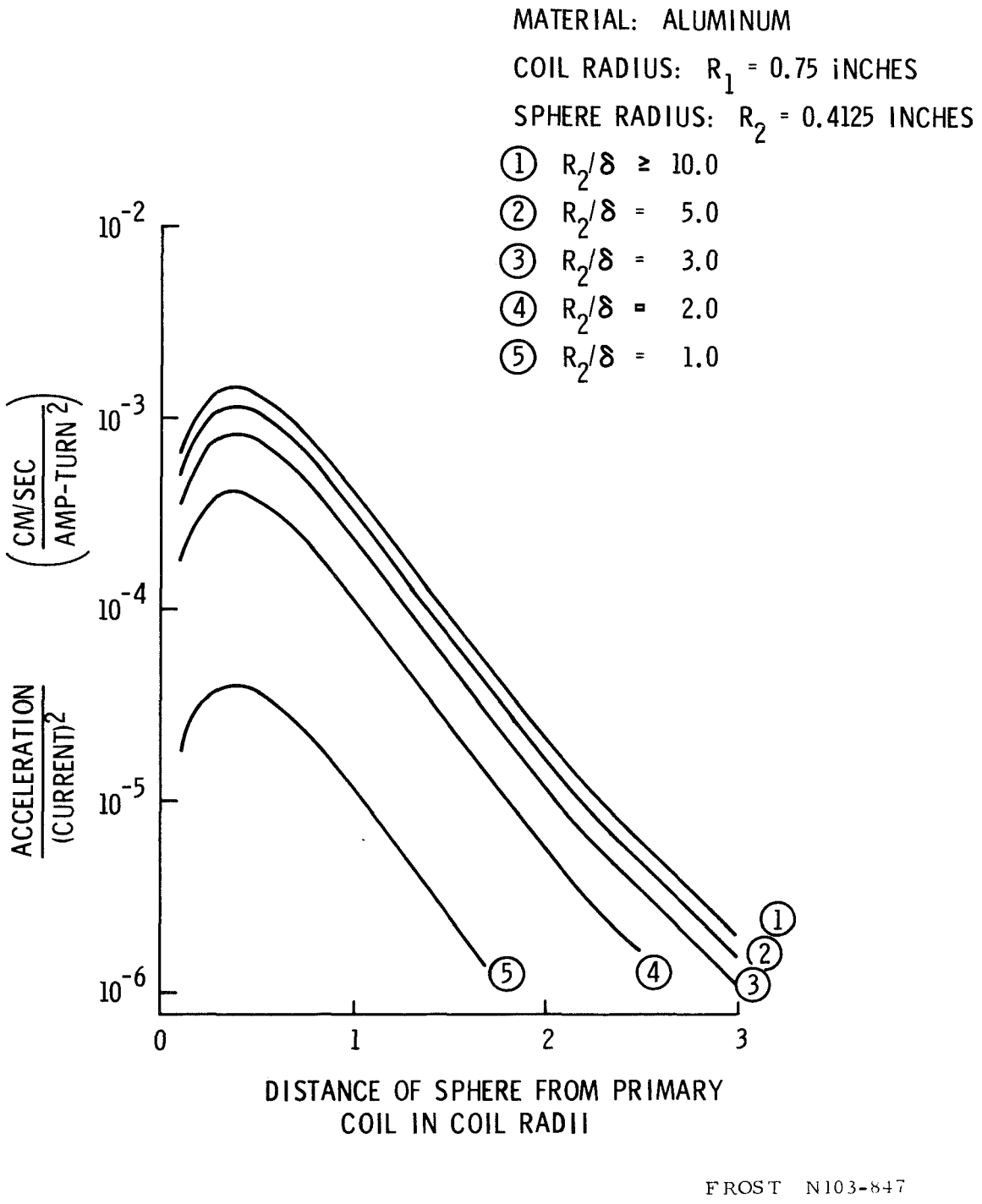

Figure IV-10. Acceleration per Unit Exciting Coil Current Squared

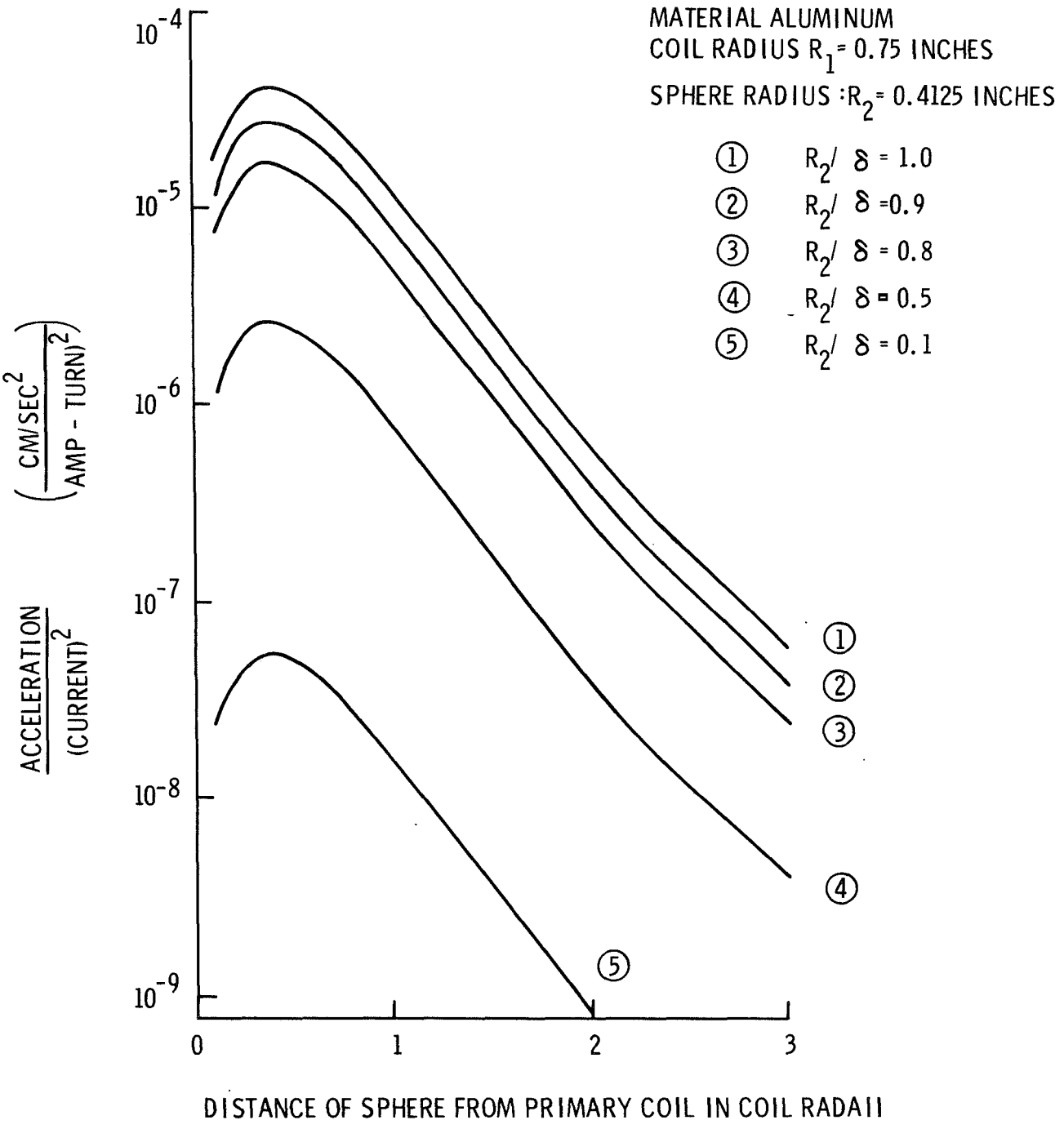

Figure IV-10A. Acceleration per Unit Exciting Coil Current Squared

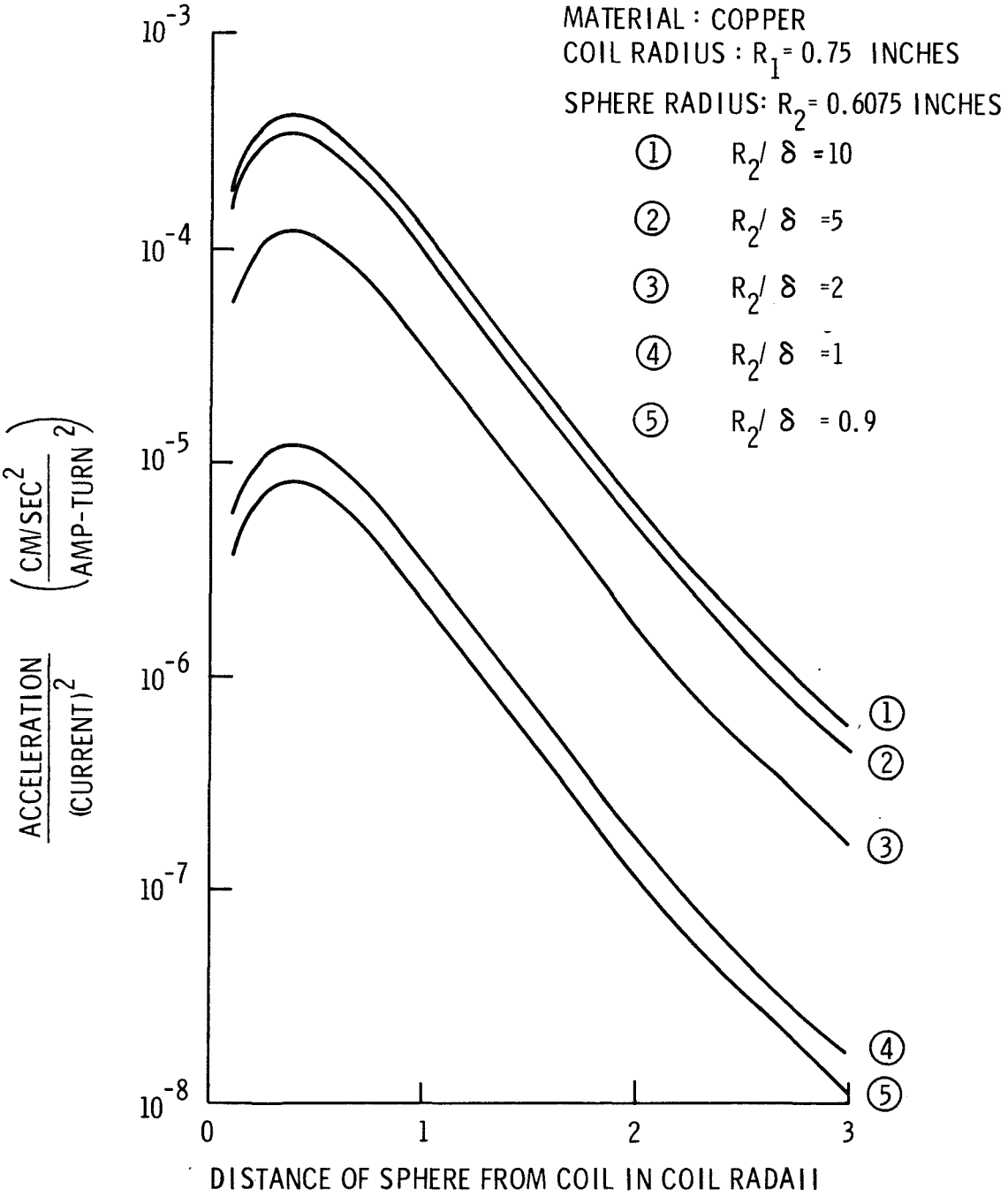

Figure IV-11. Acceleration per Unit Exciting Coil Current Squared

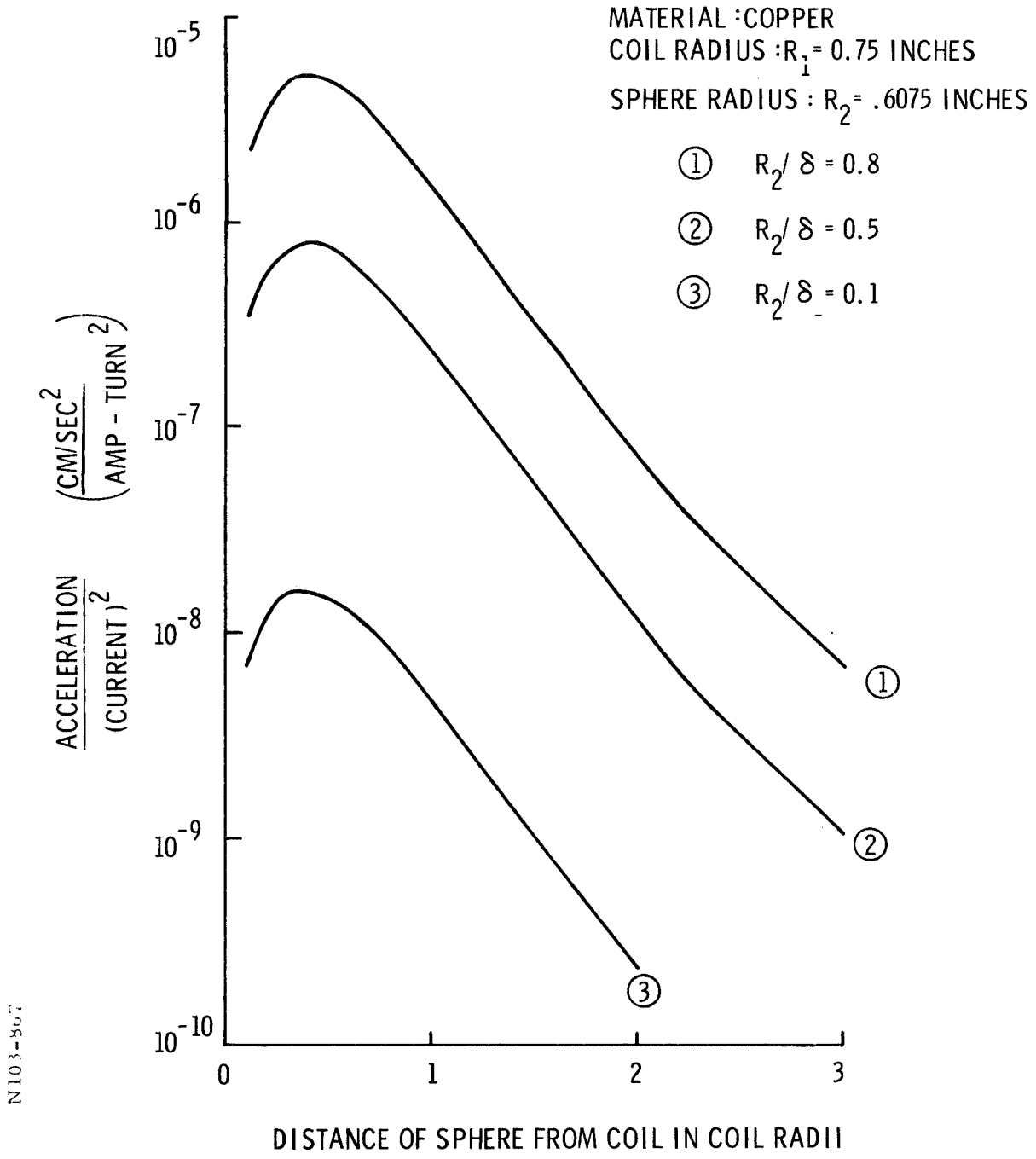

Figure IV-11A. Acceleration per Unit Exciting Coil Current Squared

V. FORCE MEASUREMENTS AND TECHNIQUES

Force-of-repulsion measurements were made to support calculations on the fundamental physical phenomena and the electronic circuitry. It is important to make actual measurements in addition to calculations because of nonlinearities, which will be discussed later. Since the electromagnetic forces depend upon the square of the field amplitude, the forces due to the separate positioning coils will not add linearly but will depend, in a complex way, on the relative phase of excitation of the coil pairs. These force measurements fall into two categories: (1) large forces obtained in a general survey, and (2) small forces of the order of dynes, which are closer to the positioning forces actually anticipated in zero-gravity materials processing experiments.

A. Measurement of Large Forces

A simple, magnetically damped beam balance was modified to support any one of several spheres above a coil of wire, as shown schematically in Figure V-1. The coil was raised and lowered to vary the spacing between the coil and sphere. The sphere was relatively motionless as the balance was returned to a balanced condition for each position of the coil. The circuit employed to pass current through the coil is also shown in Figure V-1. The 10 kHz signal from the signal generator was amplified by a power amplifier and applied to the coil, variable capacitor and one ohm resistor connected in series. The capacitor was set to tune the combination to the applied frequency and the resulting current was observed by reading the voltage generated across the resistor. With this apparatus forces were measured for several different coil-to-sphere distances (center-to-center) for each of several spheres with a limiting accuracy of approximately ± 30 dynes. Materials employed for the spheres were copper, aluminum, Inconel, Dowmetal and tungsten-carbide steel. Results for copper and aluminum at a coil current level of 1.4 rms ampere are given in Figure V-2 with the forces normalized to one ampere turn.

The same apparatus was used to obtain the data given in Figures V-3 and V-4, which are similar to those in the preceding figure except that a different coil was used and data for three different frequencies are show, viz. 10 kHz, 1kHz and 100 Hz. The currents used were about 0.2 rms ampere for 10 kHz and about 0.7 rms ampere for 1 Hz and 100 Hz. The broken lines in Figures V-3 and V-4 are the results of calculations based upon the assumption that currents within the sphere are excited by a uniform oscillating magnetic field. There is some inconsistency in computing the net translational force for the case in which the applied field is uniform. This partially explains the discrepancy shown in the figures. If the field was uniform no net force would exist. The procedure used in the calculation was to compute the currents in the sphere for the case of the uniform field and to assume that these currents were acted upon by the actual field near the coil so that a net force was obtained.

B. Measurement of Small Forces

A piece of plate glass 0.5 inch thick, 2 feet long and 1 foot wide was equipped with three micrometer screw heads which permitted controlled tilting of the glass in one direction in increments of 3.9×10^{-5} radian for each 0.001 inch division. The vernier micrometer heads allowed

tilt measurements to one-tenth of this value or 3.9×10^{-6} radian. A transparent box approximately 45 inches tall was placed on the glass plate and the same aluminum sphere as used previously was suspended from the top of the box by a fine wire, see Figure V-5. The same coil as used previously, see Figures V-3 and V-4, was placed near the sphere to obtain the data given in Figure V-6 at 10 kHz. The procedure used with the apparatus was to observe the position of the sphere on the reticle of a telescope, tilt the table a small amount, and apply current sufficient to return the sphere to its original position. The amount of tilt and the mass of the sphere indicated the force required and the current in the coil was read as described above. The accuracy of the force measurements with this technique is approximately $\pm$ 0.5 dyne, and most of this uncertainty is provided by the limit to which the position of the sphere may be read. Swinging of the sphere, which hampered observation of the sphere's position, was eliminated by attaching a lightweight probe to the bottom of the sphere in line with the wire supporting it. The probe extended about 1/8 inch into some 2,000 centistoke silicone oil. This produced a degree of damping somewhat less than critical. By taking vertical "slices" of the data of Figure V-6 the information shown in Figure V-7 was obtained.

This tilt-table apparatus was also used to measure small forces applied to spheres as they roll on an optically flat piece of glass. This technique has not yet been used but the sensitivity is expected to be no greater than $\pm$ 0.5 dyne and under ideal conditions may be as low as $\pm$ 0.05 dyne. The advantage of such a technique is to permit the sphere to range over a wider area, unrestrained by any supporting wire. A disadvantage is that a nearly perfect sphere and dust free surfaces are required.

C. Measurement of Stability of Sphere Position Within Positioning Coils When Servo Loop is Inactivated

Since the force between a given positioning coil and the floating conducting mass is repulsive, the force fields of three orthogonal pairs of positioning coils will create a potential-well centered about the common intersection of their axes when all coils are excited. A two dimensional analog of this potential well has been examined by exciting two orthogonal coil sets whose axes were horizontal. The conducting aluminum sphere was suspended on a long pendulum. The arrangement was such that, with the coils deactivated, the ball was positioned at the intersection of the two coil-pair axes. With the coils activated, oscillations of the sphere were initiated by physically touching the ball. With the two members of each coil pair connected in phase or 180° out of phase, a potential well was observed having a pincushion shape. This means that the oscillations were of lower amplitude when they were parallel to either coil-pair axes than when the plane of the oscillations made an angle of 45° with both coil-pair axes. The period of the pendulum of course depended upon both the plane of oscillation and the amplitude and ranged between 1.5 to 2.0 seconds. The natural frequency of the pendulum ($\sim$ 10 feet long) was 3.5 seconds. With the members of coil pairs connected in phase very little restoring force was apparent for ball positions near the well center and the nature of the oscillations were to some extent comparable to the case where the potential well would be a box with rather stiff reflecting boundaries. With the coils connected out of phase, the restoring forces had a "softer" nature thus demonstrating the nonlinearity of force addition. It

is well known that the axial field near the center of the Helmholtz coil pair varies approximately with the cube of the displacement from the center position. This would give a force varying as the 6th power of displacement from the center and would be qualitatively similar to the force variation observed with the coils connected in phase.

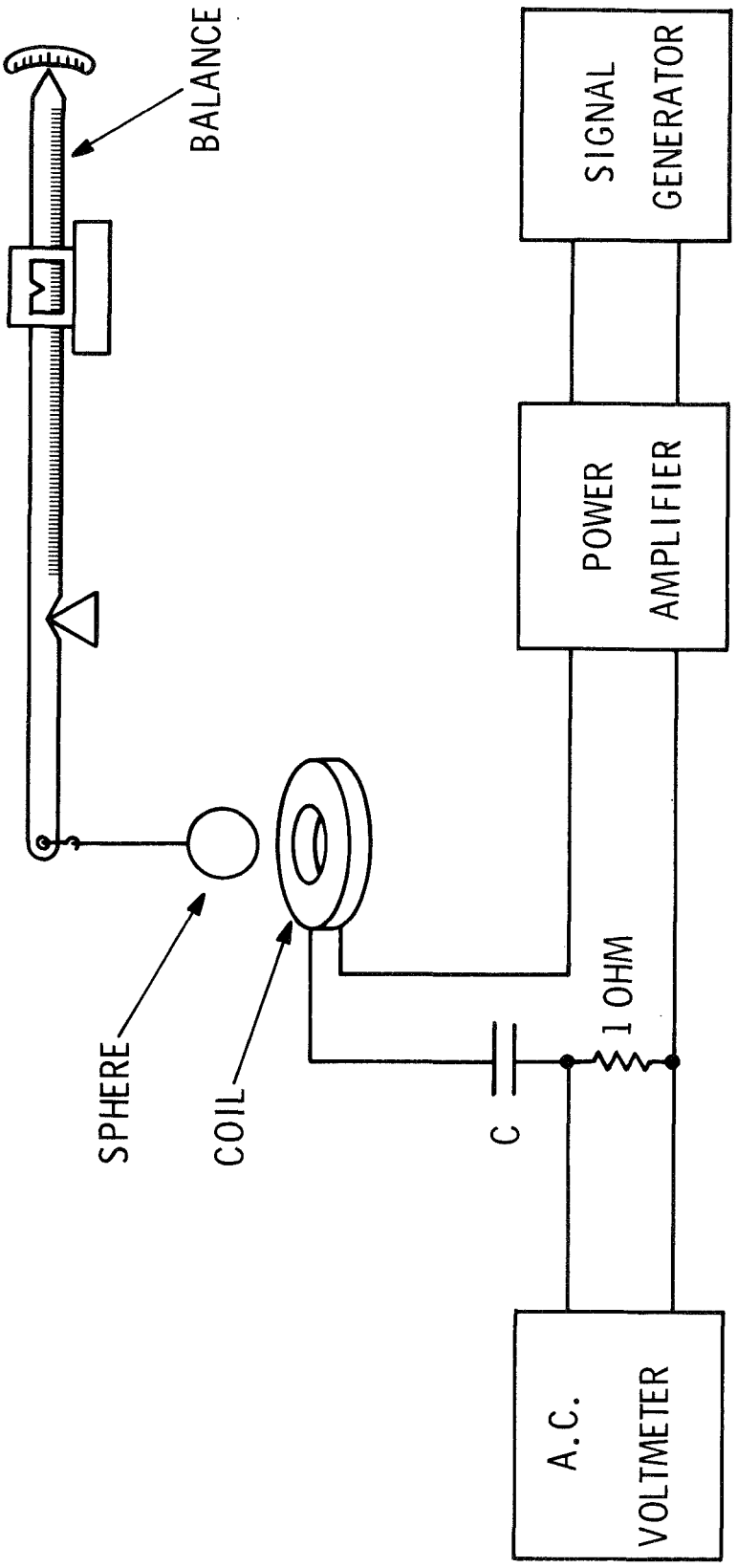

Figure V-1. Large Force Measuring Apparatus

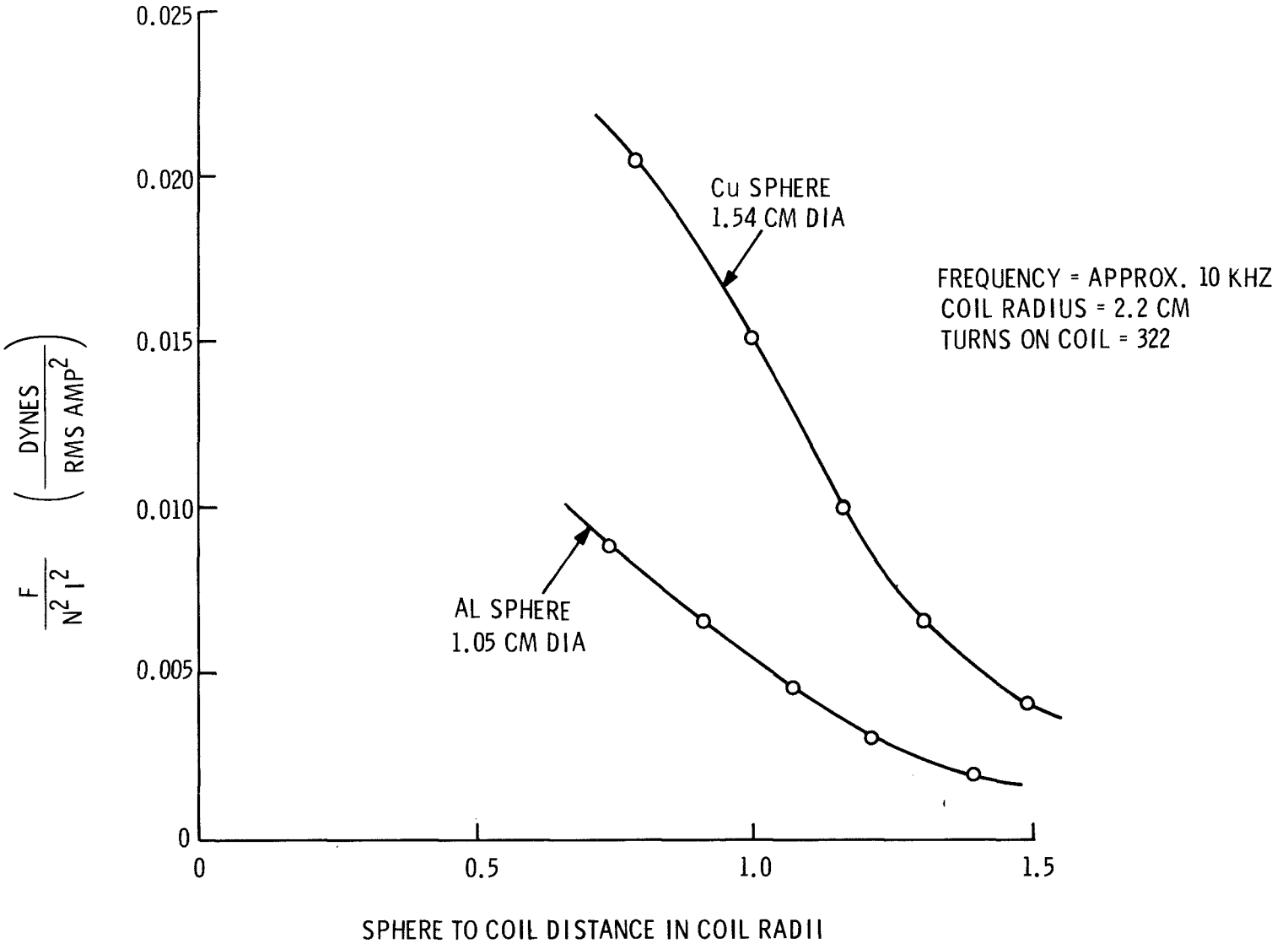
0.025
0.020
0.015
0.010
0.005
0
0
0.5
1.0
1.5
$\frac{F}{N^2 I^2}$ $\left(\frac{\text{DYNES}}{\text{RMS AMP}^2}\right)$
Cu SPHERE
1.54 CM DIA
AL SPHERE
1.05 CM DIA
FREQUENCY = APPROX. 10 KHZ
COIL RADIUS = 2.2 CM
TURNS ON COIL = 322
SPHERE TO COIL DISTANCE IN COIL RADII

Figure V-2.

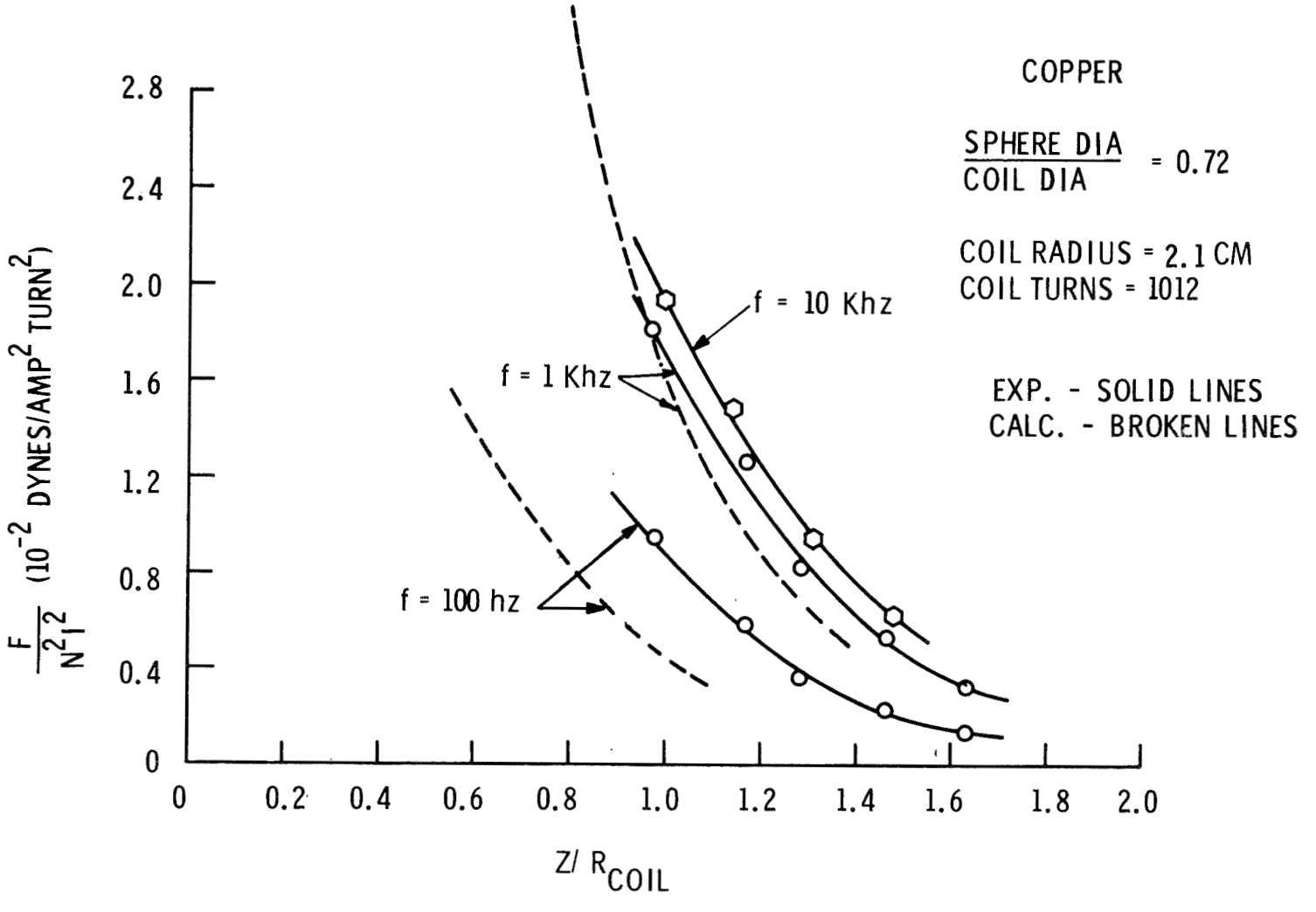
COPPER
SPHERE DIA / COIL DIA = 0.72
COIL RADIUS = 2.1 CM
COIL TURNS = 1012
EXP. - SOLID LINES
CALC. - BROKEN LINES
f = 10 Khz
f = 1 Khz
f = 100 hz
F / N²I² (10⁻² DYNES/AMP² TURN²)
Z/ R COIL
0
0.4
0.8
1.2
1.6
2.0
2.4
2.8
0.2
0.4
0.6
0.8
1.0
1.2
1.4
1.6
1.8
2.0

Figure V-3.

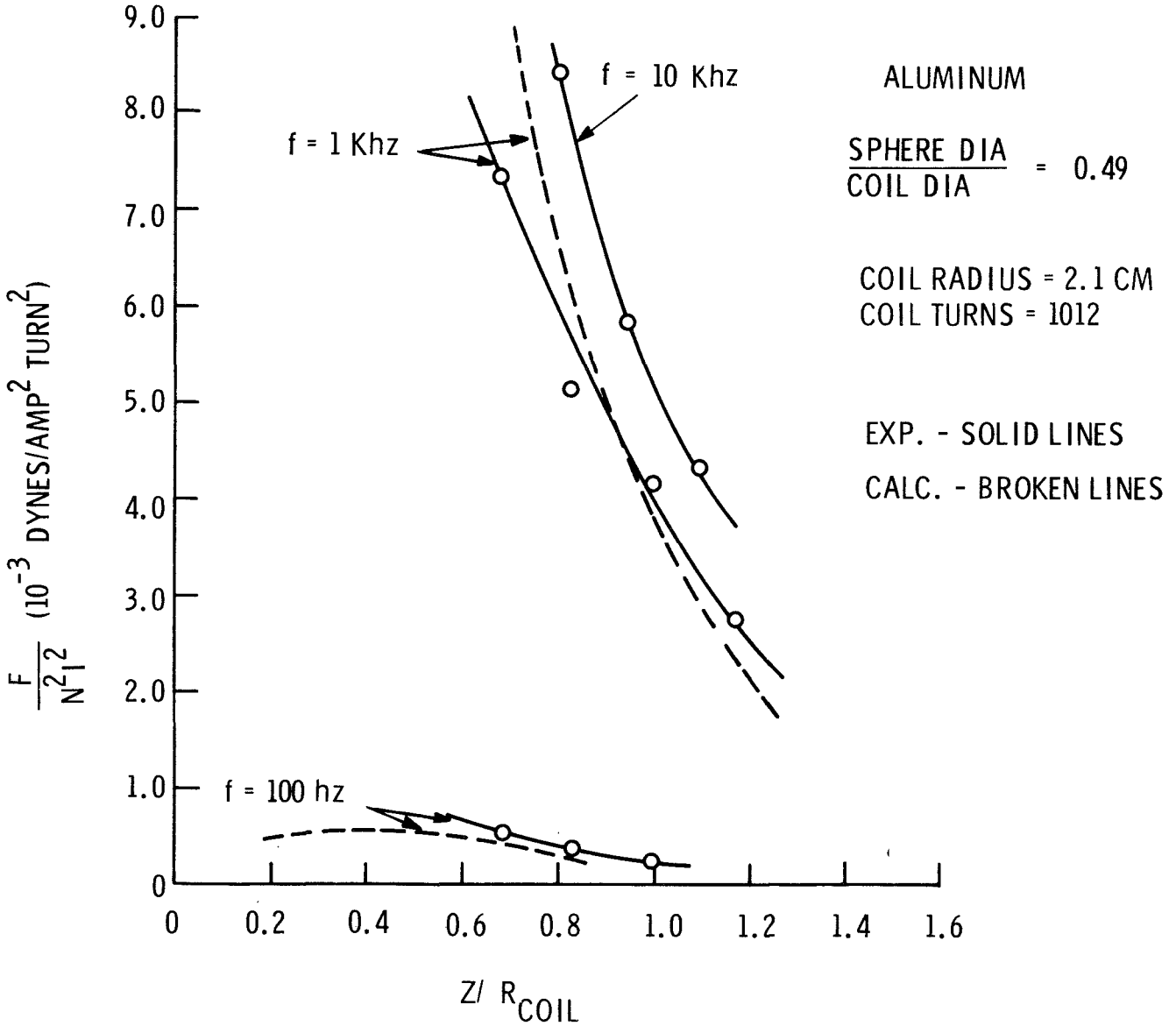
9.0
8.0
7.0
6.0
5.0
4.0
3.0
2.0
1.0
0
0
0.2
0.4
0.6
0.8
1.0
1.2
1.4
1.6
f = 10 Khz
f = 1 Khz
f = 100 hz
ALUMINUM
SPHERE DIA / COIL DIA = 0.49
COIL RADIUS = 2.1 CM
COIL TURNS = 1012
EXP. - SOLID LINES
CALC. - BROKEN LINES
F / N²I² (10⁻³ DYNES/AMP² TURN²)
Z/ R COIL

Figure V-4.

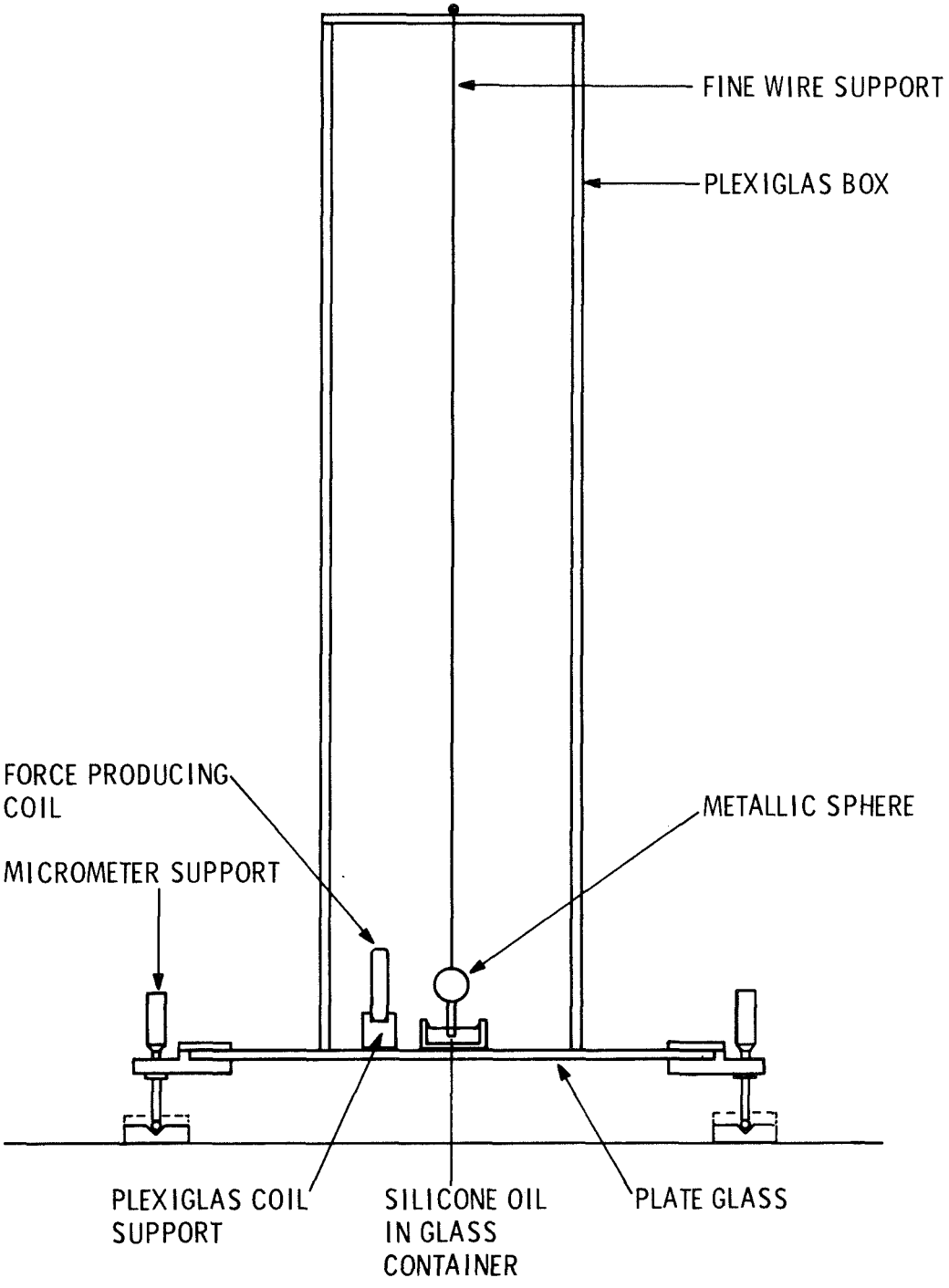

Figure V-5. Tilt Table Assembly for Measurement of Small Forces

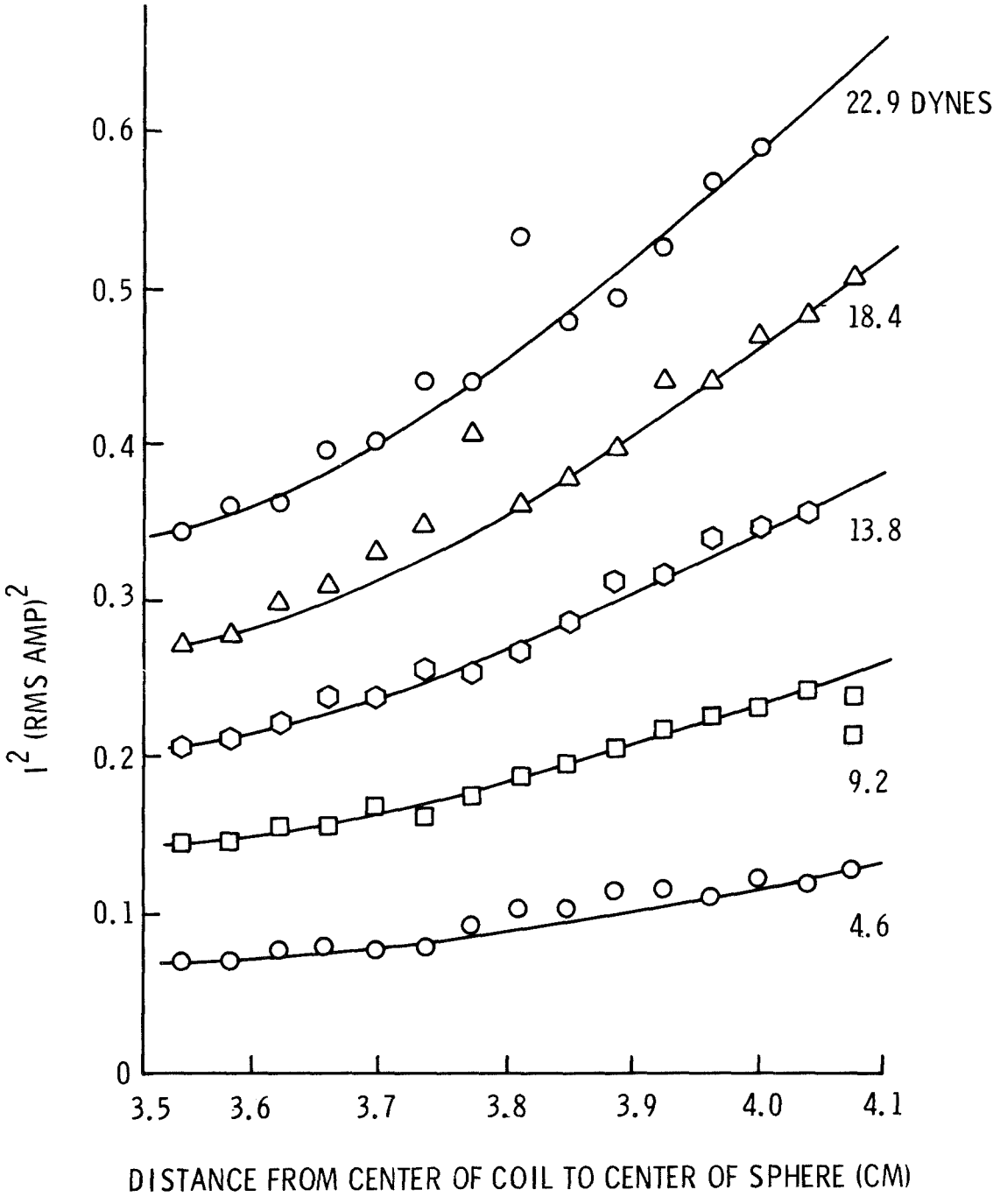

Figure V-6. Coil Current vs. Position for Constant Force at 10 Khz on Aluminum Sphere

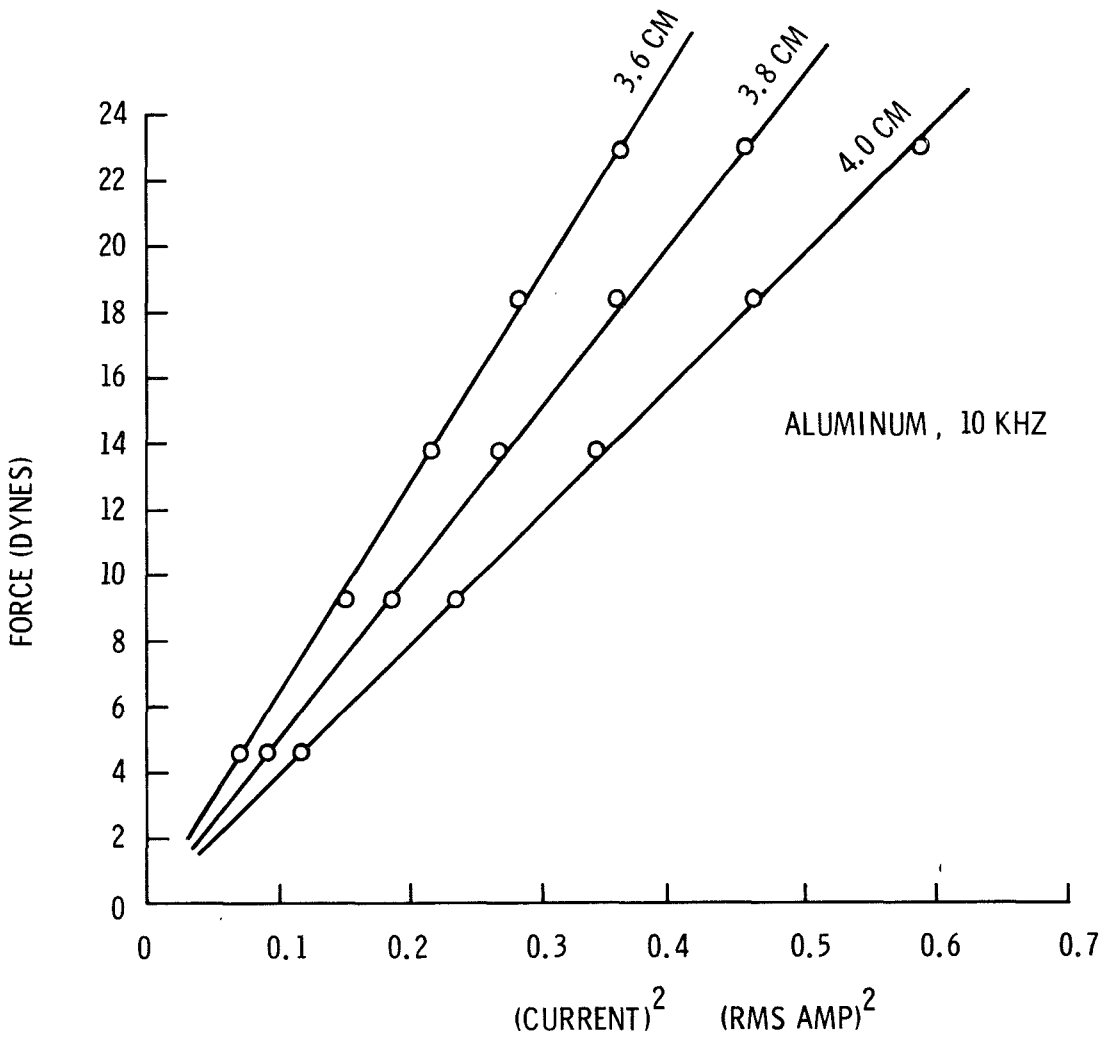
3.6 CM
3.8 CM
4.0 CM
ALUMINUM, 10 KHZ
FORCE (DYNES)
24
22
20
18
16
14
12
10
8
6
4
2
0
0
0.1
0.2
0.3
0.4
0.5
0.6
0.7
(CURRENT)^2 (RMS AMP)^2

Figure V-7.

VI. POSITION SENSING AND CONTROL SERVO

The control system hardware for position and damping is illustrated in Figures VI-1 and VI-2. Figure VI-3 is a block diagram showing details of the electronics employed in the loop (single axis) and the signal flow paths. The operation of the loop is as follows.

The coils shown at the left of Figure VI-3 are accompanied by shunt resistors which provide a signal proportional to coil current. The excitation voltage and the current signals are amplified individually and drive zero cross-over circuits in the logic block. The output of the logic circuit is a series of pulses which drive the switches, one coil switching (+) reference and one coil switching (-) reference into two summers. The duty cycle of the switches is proportional to the phase angle between the current in the coil and the excitation voltage. This phase angle is related to the position of the ball relative to the coil, as shown in Figure VI-4. Therefore, if the ball is centered between the coils, the coils have identical phase shifts and the (+) and (-) reference switches have equal duty cycles. The resultant average seen by the error summers is zero. Also, the multiplier outputs are equal and both coils have identical excitation voltages from the power amplifiers. The conditions up to now indicate a quiescent state with no disturbances to the ball.

Assume the ball occupies a position nearer to the coil shown in the upper channel of Figure VI-3. From Figure VI-4 we find this coil's current to be shifted up in phase and the lower coil, which is further from the ball, is shifted down in phase. Under these conditions the (+) reference switch duty cycle decreases and the (-) reference switch cycle increases. The error in the upper channel becomes (+) at the summer output (the summer inverts) and the modulator increases the signal to the power amplifier and the upper coil. This acts to repel the ball back toward the center position. Even though the lower summer's output goes (-), the modulator is so biased and driven that its output does not go much below the level it has when the ball is at the quiescent position. This ensures the presence of a minimum signal from which to get phase and hence position information from that coil.

So far, discussion has been confined to the static properties of the control system. The individual elements of the system shown in Figure VI-3, in general, take a certain time to react, or more accurately, the transient behavior is some function of time. Looking at the position sensing first, we find that phase angle relates to position. The phase angle is sampled and summed each half cycle so that at 10 kHz, position data lags position by about 25μ seconds. The voltage and current amplifiers have no delay networks and in fact have several MHz bandwidths. To reduce ripple in the position information, ripple filters are employed at the summers and at the modulators. The value of their cut-off frequencies are determined by allowable ripple and loop bandwidth. Representative values are 300 or 400 Hz for a 100 kHz operating frequency.

The summers contain, in addition to a ripple filter, a lead network which is required for damping the loop. This lead network has associated with it a lag at a frequency of about ten times the lead

frequency. The exact frequency of the lead network is determined by the gain and bandwidth requirements for given load dynamics, the value in this case being about one Hertz.

The last electronic time constant belongs to the resonated coil which at 10 kHz has a Q of about 25 and therefore a frequency bandwidth of about 400 Hz. The final dynamic consideration is the load, in this case the sphere of mass m. The coil exerts a force $f = ki^2$ for small signals so the change in force per change in current is $2 ki \nabla i$. We see immediately the square law property of the force which means the overall loop gain is proportional to the current. At a given current, however, the force can be represented by $k' \nabla i$. The transfer function of a mass without viscous force is simply $X(s) = f(s)/ms^2$, where x represents distance. This signifies a double lag (-40 db per decade) passing through the point 1/m at 1 radian per second.

From the above, it is seen that there is no viscous damping so it is necessary to provide damping in the control loop. This necessity is met by the lead which is placed at the summer. In addition to these transient responses of the various elements each element has a static gain. The electronic gains, once set, are fixed but the position sensing and replusion forces vary. Figures VI-4 and V-7 show the relations between phase angle and position and between force, current and position. The most variable element is the force which is not only a function of i^2 but of the axial distance between coil and ball. Therefore, the loop characteristics must be determined for a range of static gains. Assuming that the ball stays reasonably well centered in the present loop this gain variation nominally is about 10 to 1, the higher gain being with the ball deliberately decentered causing a high coil current to flow.

A deviation in these dynamic and static gains occurs when the mass is a pendulum bob, as shown in Figure VI-5. This deviation is due to a different load transfer function which now is affected by a gravity induced restoration force and its attendant natural frequency of vibration. This transfer function for the pendulum mass is $X(s) = f(s)/m[s^2 + g/Lm]$, where L is the pendulum length.

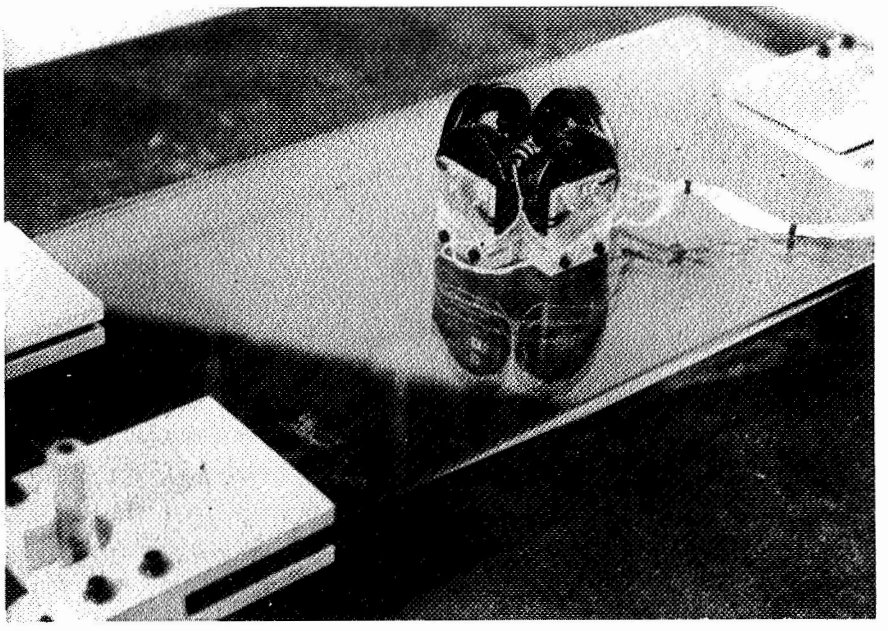

Figure VI-1. Positioning Coils on Tilt Table

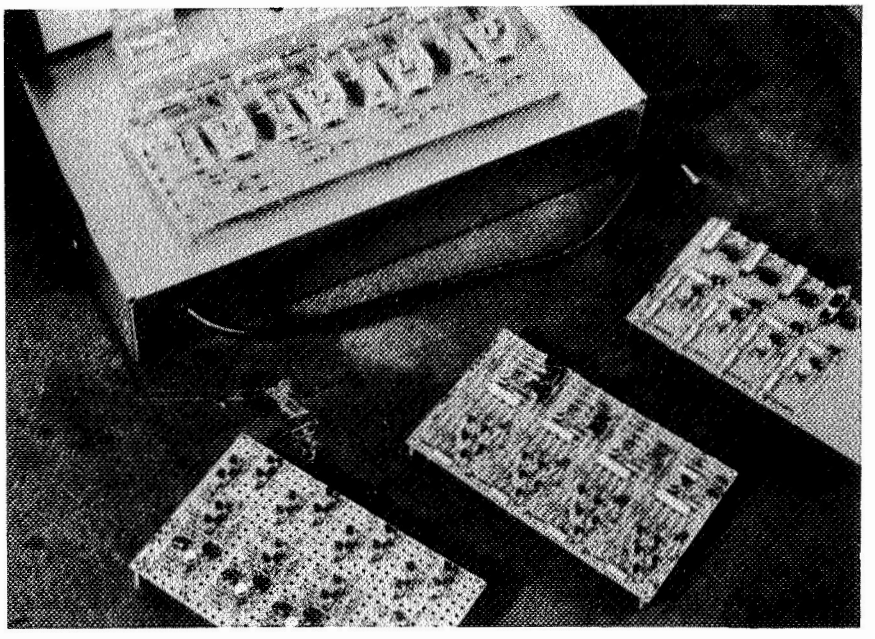

Figure VI-2. Electronic Breadboards for Position Servo

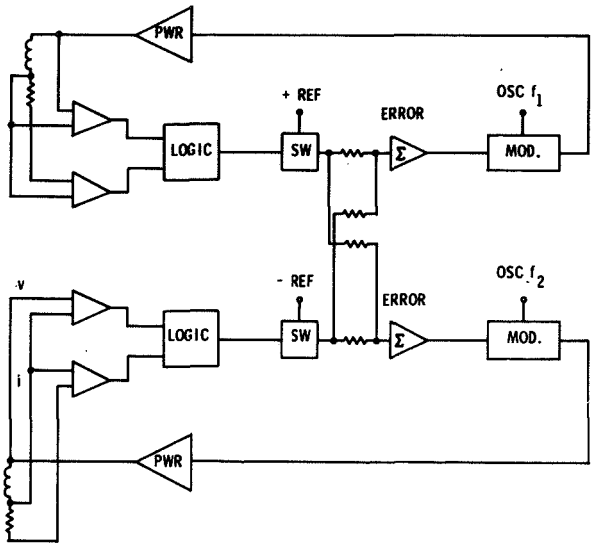

Figure VI-3. Block Diagram of Position Servo Electronics

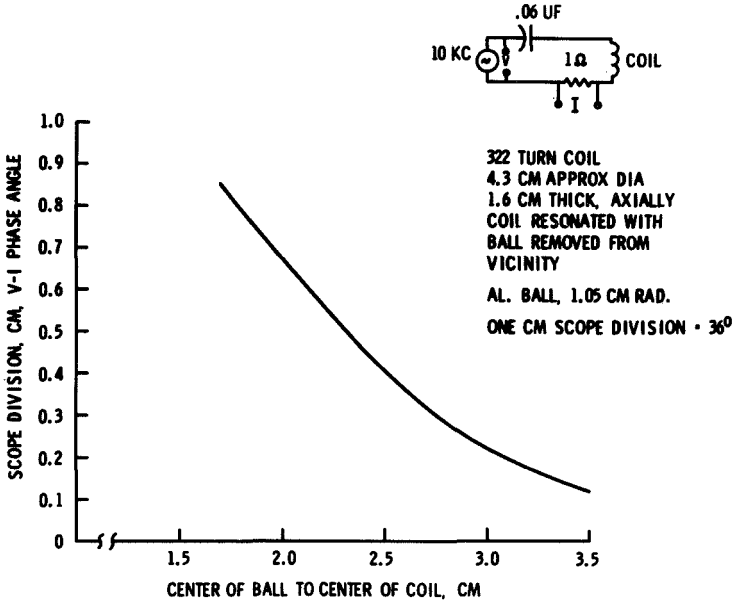

Figure VI-4. Position Sensing Characteristic

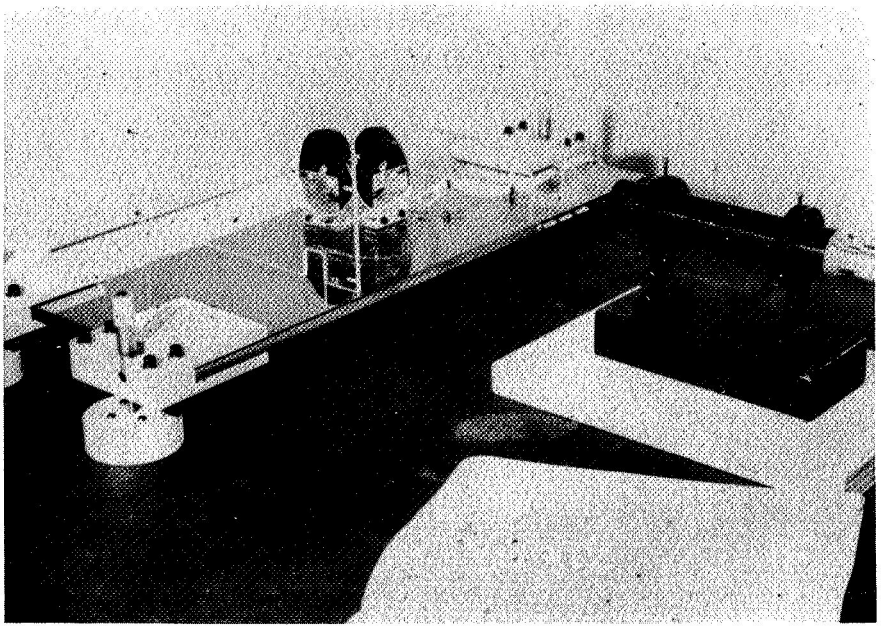

Figure VI-5. Force Measuring Apparatus Tilt Table and Pendulum

VII. MATERIAL PROPERTIES – GENERAL CONSIDERATIONS

A. Electric and Magnetic Properties

When considering the properties of conductors and dielectrics we must consider the form of Maxwell's equations within a material medium. The equation relating magnetic field intensity and current for linear, isotropic nonpermeable media can be written as

$$\nabla \times (\mu_o \vec{H}) = \mu_o \vec{J} + \mu_o \kappa_e \epsilon_o \, \partial \vec{E} / \partial t \ ,$$

or

$$\nabla \times \vec{B} = \underbrace{\mu_o \vec{J}}_{\text{Conduction Current}} + \underbrace{\mu_o \kappa_e \epsilon_o \, \partial \vec{E} / \partial t}_{\text{Displacement Current}} \ .$$

in the M.K.S. system of units, where $\mu_o = 4\pi \times 10^{-7}$ henry/meter and is the permeability of free space, $\epsilon_o = 8.854 \times 10^{-12}$ farad/meter and is the permittivity of free space, and κ_e is the relative permittivity of the linear, isotropic, homogenous, nonpermeable medium.

In a good conductor

$$\mu_o \vec{J} >> \mu_o \kappa_e \epsilon_o \, \partial \vec{E} / \partial t \ ,$$

and in a poor conductor

$$\mu_o J << \mu_o \kappa_e \epsilon_o \, \partial E / \partial t \ ,$$

so that ratio

$$Q = \frac{\mu_o \kappa_e \epsilon_o \, \partial \vec{E} / \partial t}{\mu_o \vec{J}}$$

is a quantity which expresses the importance of conduction currents or displacement currents in a material. For a time harmonic field $\vec{E} = \vec{E} e^{j\omega t}$, and $\partial \vec{E} / \partial t = j \omega \vec{E}$, so with $\vec{J} = \sigma \vec{E}$ the ratio Q is just $\kappa_e \epsilon_o \omega / \sigma$.

The quantity 1/Q is the ratio of conduction to displacement currents. In a good conductor like copper 1/Q will range from 10^{17} to 10^{12} as the frequency increases from 10 to 10^6 cps., while in a cold glass 1/Q will range from 10^{-3} to 10^{-9} over the same range of frequencies. Figure VII-1 shows the range of 1/Q's possible in the frequency range 10^3 to 10^6 cps. for a molten glass. Here the range of conductivities is 1 mho/meter to 10^4 mho/meter, and taking a typical permittivity of $\kappa_e = 5$ (data show κ_e can vary from 3 to 18) the range of $\sigma/\kappa_e \epsilon_o$ is 2.26×10^{10} to 2.26×10^{14} and values of 1/Q within this rectangular region will range from about 1.59×10^4 to 1.59×10^{10}. It can be seen that as we go up in frequency the quantity 1/Q decreases, since here displacement currents are becoming more and more important. We can also conclude that within this frequency band conduction currents still dominate appreciably. For intermediate temperatures, the conduction and displacement currents in glass will become of comparable magnitude.

B. Skin Depth

Electromagnetic waves of any frequency (greater than those which might better be called slowly varying d c fields) falling upon a conducting material of zero resistivity would behave as light falling upon a mirror; all of it would be reflected. If the conducting material has a non-zero resistivity, then the electromagnetic waves penetrate the material, loosing energy in the process, and the depth by which the amplitude of the wave has dimished to 1/e or 0.37 of its initial value is the attenuation distance or the skin depth. This skin depth, δ, depends upon the properties of the material and the frequency of the wave as follows:

$$\delta = \frac{1}{\sqrt{\pi \, f \, \sigma \, \mu}} \quad ,$$

where f is the frequency of the wave in cps or Hz, σ is the conductivity of the material in mhos/meter (one mho/meter is equivalent to a resistivity of 100 ohm-cm), μ is the magnetic permeability of the material in Newtons/ampere^2($\mu = 4\pi \times 10^{-7}$ Newton/ampere^2 if the relative permeability is unity) and δ is the skin depth in meters. The skin depth has been plotted in Figure VII-2 for several materials and a wide range of frequencies. Here it may be noted that the skin depths achieved in aluminum and copper in work discussed elsewhere in this report ranged from 0.8 cm at 100 Hx to 0.5 mm at 10 kHz.

C. Melting Power Required to Supply Surface Radiated Power Loss

Table VII-1 presents the melting points of various materials, the power required to overcome radiation loss at the melting point, and the total power required for a sphere of 10 cm^2 surface area. This is an important factor in selecting materials for experimentation and in designing apparatus to melt these materials.

TABLE VII-1

Substance or Element	T Melt (C)	T Melt (^{o} K)	T Melt (^{o} K)^4	Surface radiation loss for 10 cm^2 and unity emissivity*
T_i	1800^{o}C	2073.16	18.473 x 10^{12}	1.04 x 10^3
Be	1283^{o}C (Top)	1556.16	5.864 x 10^{12}	3.32 x 10^2
Zr	1857^{o}C	2130.16	20.590 x 10^{12}	1.17 x 10^3
W	3370^{o}C	3643.16	176.162 x 10^{12}	1.00 x 10^3
M_o	2620^{o}C	2893.16	21.895 x 10^{12}	3.97 x 10^3
C_r	1890^{o}C	2163.16	21.895 x 10^{12}	1.24 x 10^3
T_a	2996^{o}C	3269.16	114.221 x 10^{12}	6.47 x 10^3
PbTe	917^{o}C	1190.16	2.006 x 10^{12}	1.13 x 10^2
Steel	1537^{o}C (Top)	1846.16	11.617 x 10^{12}	6.58 x 10^2
Ni	1455^{o}C	1728.16	8.919 x 10^{12}	5.05 x 10^2
Ga	29.78^{o}C	302.94	84.222 x 10^8	.48

* σ = 5.668 x 10^{-12} watts/cm^2 (^{o} K)^4

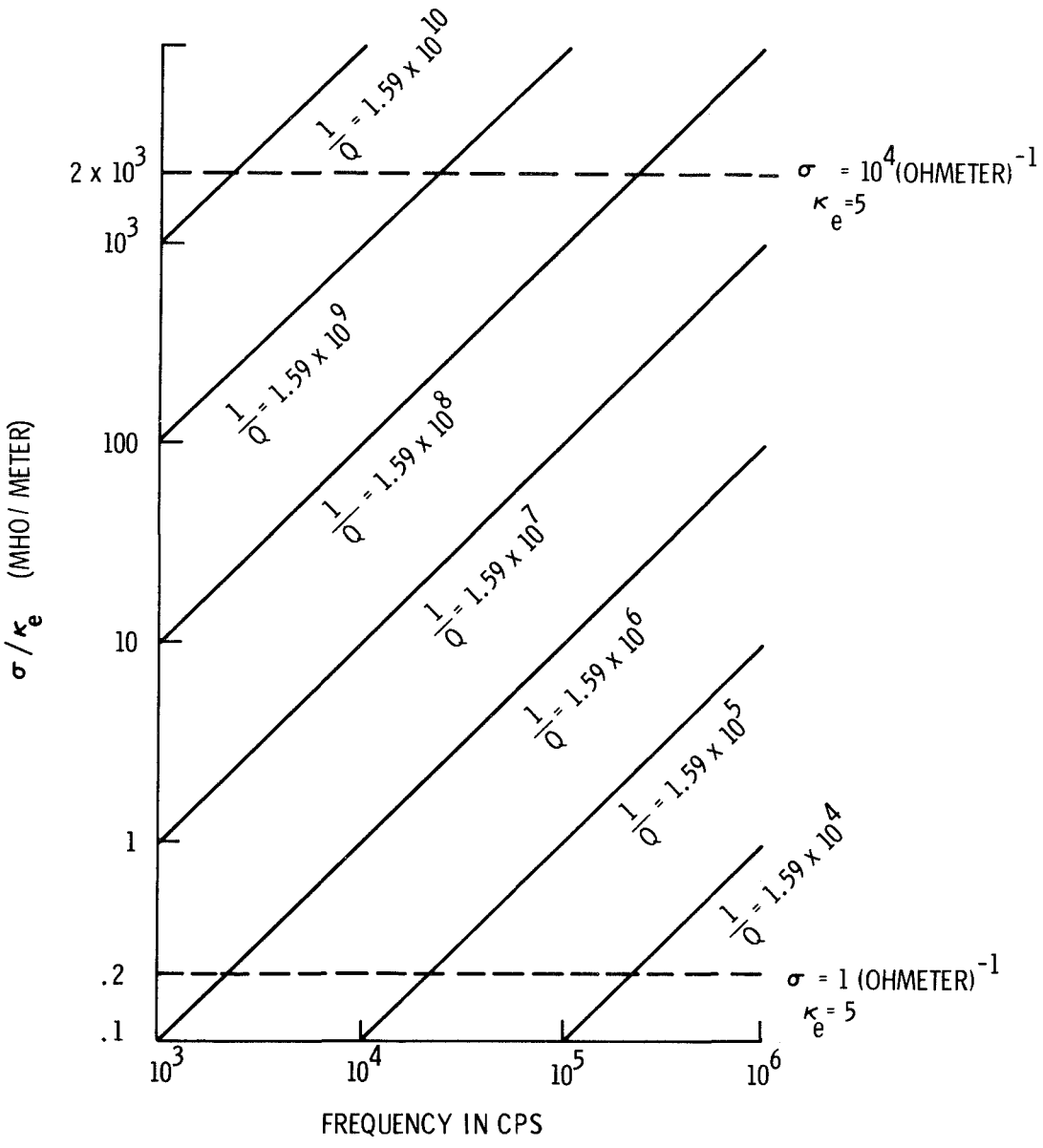

Figure VII-1. Plot of $\rho/\kappa_e\epsilon_o = (2\pi/Q)f$ with Dashed Lines a Molten Glass Region

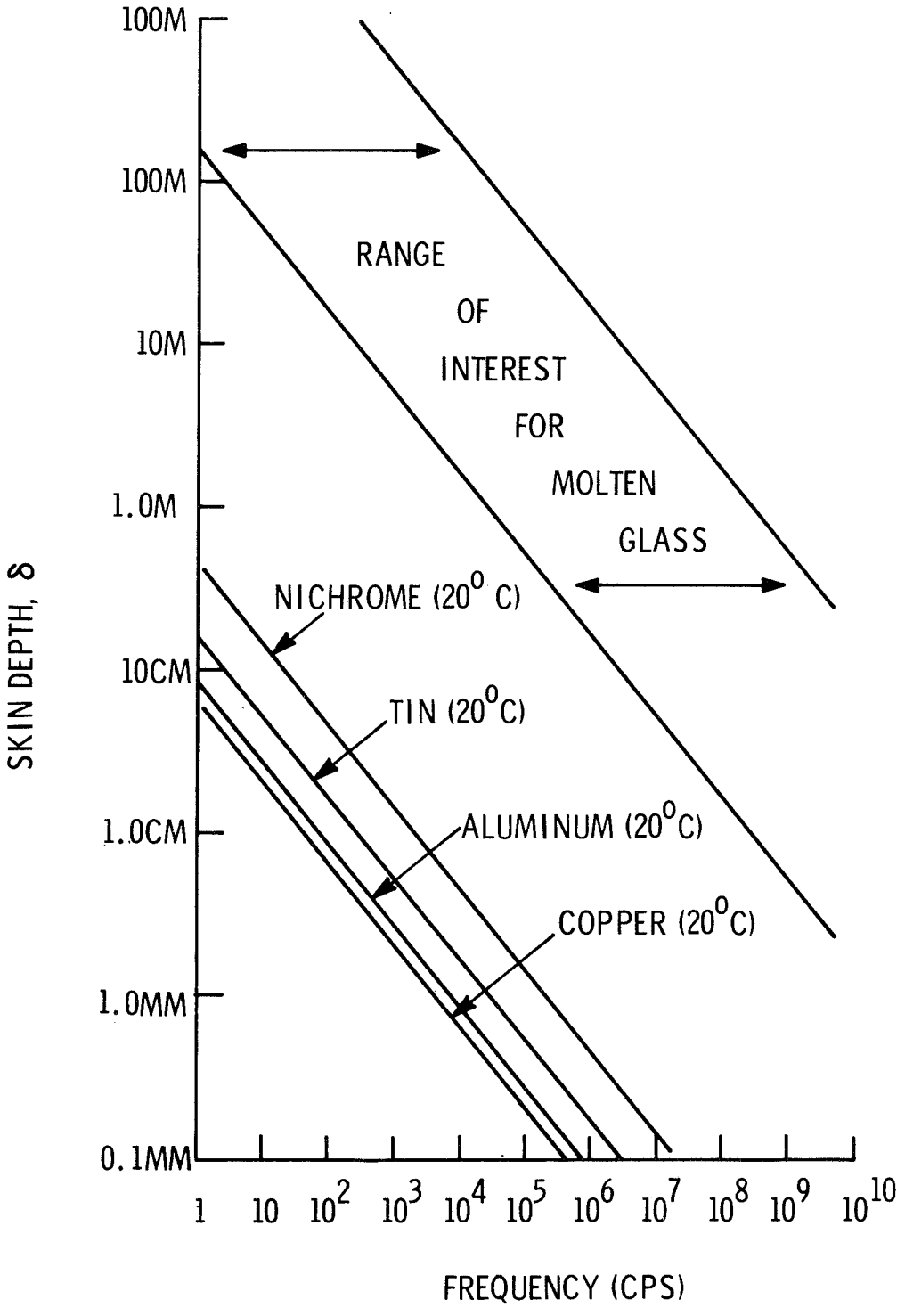

Figure VII-2. Skin Depth vs. Frequency for Several Common Metals and Molten Glass

VIII. HYDRODYNAMIC CONSIDERATIONS

A. Introduction

We have begun work on the problem of the oscillatory, rotational, and translational motions of a fluid body under the influence of electromagnetic field forces. The problem can be broken up into the following areas:

(1) Oscillations of a stable fluid body shape

(2) Determination of possible stable shapes of fluid bodies within electromagnetic fields

(3) Fluid currents within fluid bodies of stable shape

(4) Translatory motions of fluid bodies and the changes in shape under the action of translatory forces.

A few basic problems have been considered which have applicable results and can be extended to more complex problems.

B. Oscillations

1. Excitation or Damping by Positioning Device

Excitation of the position control coils can be used either to initiate or damp translational motions of the floating mass and shape oscillations as well as any rotations which may occur. The position control and shape oscillation problem is most easily treated by considering individual hydrodynamic modes of a liquid sphere under the action of surface tension forces and the electromagnetic forces due to internal eddy currents.

Figure VIII-1 illustrates the first three hydrodynamic modes. We can describe these modes most easily by expressing the distance from the center of mass to the liquid surface r as a function of a colatitude θ in the way shown at the bottom of the figure. For the zero mode, the radius vector equals a constant a_o multiplied by the 0 order Lengendre polynominal which is simply unity. For this mode the mass is a perfect sphere with no distortion modes. For the second hydrodynamic mode, which represents a shape oscillation between prolate and oblate spheroid, we must add to the original radius a term a_2P_2 (cos θ) cos $\omega_2 t$. The center drawing in Figure VIII-1 illustrates this shape at a given instant of time. The shape oscillates sinosoidally between oblate and prolate. This oscillation mode can be either excited or damped by application of the magnetostriction forces thru excitation of the position control coils. In a paper given at the MSFC Symposium last year one of

the present authors discussed the limitations arising from excitation of oscillations and showed that processing of liquid metal masses at least as large as tens of kilograms can be considered without worrying about rupture of the mass due to the necessity of position control in practical cases.

If the position control coils along a given axis are excited asymmetrically, e.g., if we excite only one, then we will obtain a net translational force which will excite both the first and third mode. The third mode resembles an eggplant and can be treated similarly to the second mode. The first mode shown as P_1 in Figure VIII-1 represents pure translation of a spherical shape and must be treated differently from the other modes. The reason for this is that the frequency corresponding to the first mode is zero and for this particular term in the sum we should replace the sinusoidal time term by a term linear in time. We have begun to examine theoretically the excitation or damping of these various models by excitation of the coils.

2. Free Oscillations

The free oscillations of a viscous liquid globe are of interest in determing the natural frequencies of the system where resonances can occur. The basic problem we consider here is a small fluid sphere of incompressible, viscous fluid under the action of surface tension alone and the small oscillations of the fluid about its spherical form. Lamb (19) had discussed this problem in detail for inviscous fluids where the shape is given by

$$r = R\,[1 + \epsilon\, Y_{\ell}^{m}(\theta, \Phi)\,]$$

for the deformations of the liquid surface where

$$\epsilon = \epsilon_0\, e^{i\sigma t} \text{ and } \epsilon << 1 \ ,$$

with frequencies of oscillation given by

$$\sigma_{\ell;\,0}{}^2 = \ell\ (\ell - 1)(\ell + 2)\, T_1/\rho R^3 \ ,$$

where $\sigma_{\ell;\,0}$ is the oscillation frequency for inviscous liquids

ℓ = the degree of the surface harmonic $Y_{\ell}^{m}(\theta, \Phi)$

R = the radius of the undeformed sphere

ρ = density of the fluid

T_1 = surface tension/unit length

$$Y_{\ell}^{m}(\theta, \Phi) = P_{\ell}^{m}(\cos\theta)\left\{ g_{\ell}^{m} \cos m\Phi + h_{\ell}^{m} \sin m\Phi \right\} \ ,$$

where the P_{ℓ}^{m} s are the associated Lengendre polynominals.

For small oscillations of viscous fluids about their spherical form the problem is to determine the $\sigma_{\ell;\nu}$'s or the frequencies of oscillation for a coefficient of kinetic viscosity ν. This involves solving the linearized equations of motion:

$$\frac{\partial \vec{u}}{\partial t} = -\nabla \frac{\delta P}{\rho} - \nabla \times (\nabla \times \vec{u})$$

$$\nabla \cdot \vec{u} = 0 ,$$

where $\vec{u}$ = velocity, P = pressure, ρ = density and t is time subject to prescribed boundary conditions which are:

(1) At the deformed surface of the drop the radial component of the velocity must be equal to the velocity of the surface itself

(2) The tangential stresses vanish at the surface

(3) The normal component of the viscous stress is $-P_{rr} = T_1 (1/R_1 + 1/R_2)$. Here R_1 and R_2 are the principal radii of curvature taken positive when directed inward.

Reid (20) has discussed this problem and he obtains the characteristic equation for the frequencies of oscillation:

$$\frac{\alpha^4}{q^4} + 1 = \frac{2(\ell - 1)}{q} \quad \ell + (\ell + 1)\left[\frac{q - 2\ell\, Q_{\ell + \frac{1}{2}}(q)}{q - 2\, Q_{\ell + \frac{1}{2}}(q)}\right]$$

where $Q_{+\frac{1}{2}}(q)$ is written in terms of spherical Bessel functions as $J_{\ell + 3/2}(q)/J_{\ell + \frac{1}{2}}(q)$.

Here we have

$$\alpha^2 = \frac{\sigma_{\ell;o} R^2}{\nu}$$

$$\frac{\sigma_{\ell;\nu}}{\sigma_{\ell;o}} = \frac{q^2}{\alpha^2} ,$$

so we can solve the characteristic equation and get the $\sigma_{\ell,\nu}$'s. Then $r = R\,[1 + \epsilon\, Y_\ell^m(\theta, \Phi)]$ and the following results are obtained:

(1) As $q \to \infty$, the limiting case of small viscosity

$$\sigma_{\ell;\nu} = (\ell - 1)(2\ell + 1)\,\nu/R^2 \pm i\sigma_{\ell;o},$$

which is Lamb's result,

(2) The characteristic equation admits solutions of two types, depending on a value of α called the critical value α_c.

(a) If $\alpha^2 > \alpha_c^2$ then damped oscillations will occur.

(b) If $\alpha^2 < \alpha_c^2$ two aperiodic modes of decay appear.

During the next quarter numerical values of the $\sigma_{\ell,\nu}$'s will be obtained for selected materials.

C. Internal Fluid Currents

In addition to generation or damping of surface oscillations and translational motions, we can stimulate circulating currents within the floating mass by magnetostrictive forces as discussed earlier. Figure VIII-2 shows a simple current pattern which can be stimulated by exciting a single control axis. These fluid currents can be oriented in various directions by exciting various sets of coils. These currents will be useful for stirring of alloys or dispersions and will also affect bubble motion in an important way.

At the higher frequencies the pressure gradient resulting from the magnetostrictive forces which drive the steady state fluid currents will be concentrated in a thin surface layer centered about the equatorial plane with respect to the excitation axis. After the coils are excited an equilibrium will be reached quickly in which this driving pressure gradient is balanced by viscous forces. At lower frequencies where the skin depth becomes an appreciable fraction of the sphere radius the flow patterns will be altered somewhat.The quasiequilibrium shape of this spheroid will be influenced not only by the magnetostrictive forces which drive the fluid currents but also by the dynamics of the circulating dense fluid. Since magnetostrictive forces can be applied in an arbitrary manner and translational acceleration of the mass can be suppressed by simultaneous excitation of opposite members in coil pairs, we see that considerable freedom exists for electromagnetic shaping of the floating mass in various symmetric or asymmetric configurations.

D. Rotation

If we consider an orthogonal pair of excitation coils to be excited with a phase quadrature so as to produce a rotating magnetic field, we can calculate that the spheroid will be caused to rotate in the

manner of the rotor of an induction motor. By proper choice of excitation for various pairs of the positioning coils, angular velocity can be imparted to the floating spheroid in any desired direction and with any speed consistent with configurational stability of the mass. This will be limited by the stability furnished by the action of surface tension. Oscillational instability can occur for higher rotational speeds and damping due to viscosity will play a key role in prevention of buildup of catastrophic oscillations. Conversely, properly phased excitation of a given pair of coils can be used to remove an angular velocity orthogonal to both coil axes if such rotation is not desired.

E. Sound Wave Generation

The high frequency variation of magnetostriction forces can be used to generate sound waves within the floating mass if we desire to go to high level excitation. This might be useful, for example, to prevent aglomeration of oxide dispersion particles within the mass as suggested by our research laboratory people.

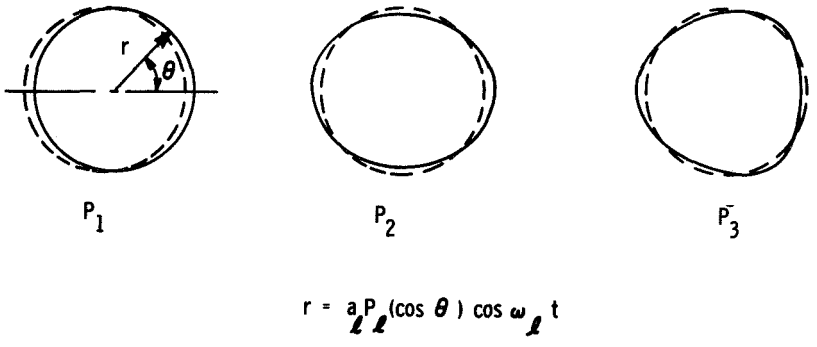

Figure VIII-1. Hydrodynamic Modes

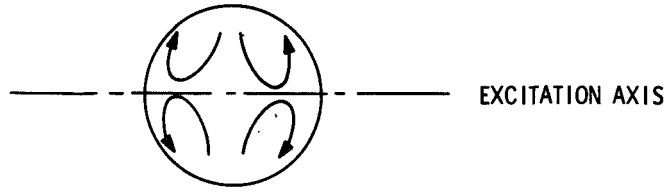

Figure VIII-2. Fluid Currents Due to Magnetrostriction

REFERENCES

1. R. Irmann, "Heat-resisting Sintered Aluminum," The Engineers Digest, **13**, 1, 9–12 (1952).

2. G. E. Wasieleuski, "Nickel-Base Superalloy Oxidation," TM 67-560, MDLO, GE Co., Cincinnati, Ohio.

3. G. E. Wasieleuski, "The Effect of Rare-Earth and Manganese Additions on the Surface Stability of Nickel-Base Superalloys," R68 AEG 430 M&P TL, GE Co., Lynn, Massachusetts/Cincinatti, Ohio.

4. G. E. Wasieleuski, "Oxidation/Hot Corrosion of Rene' 80," R68AE6216, AEG-TIS, GE Co., Lynn, Massachusetts/Cincinnati, Ohio.

5. A. Seybolt, GE R&DC, private communication.

6. R. Allen, GE, AEG, private communication.

7. F. L. Ver Snyder, "Directional Solidification in the Precision Casting of Gas Turbine Parts," Modern Casting (Dec. 1967).

8. A. J. Kiesler, GE R&DC, private communication.

9. W. F. Moore, GE R&DC, private communication

10. R. G. Hardy, "Shaped Titanium Castings," Trans. Vac. Met Conference 1960.

11. W. Moffit, GE R&DC, private communication.

12. M. Benz, GE R&DC, private communication.

13. G. Fox, "The Application of High-Purity Beryllium Conductors to Cryogenic Electric Power Apparatus," presented at the fall meeting AIME, Philadelphia, Pa. (1969).

14. "Resistive Cryogenic Cable," Phase A Report March 1969 EEI Project RP 78-6, Underground Transmission Research and Development Program, Edison Electric Institute, New York, N. Y.

15. W. R. Smythe, *Static and Dynamic Electricity,* McGraw-Hill Book Co., 396–400 (1950).

16. E. Fromm and H. Jehn, "Electromagnetic Forces and Power Absorption in Levitation Melting," Brit. J. App. Phys., **16**, 653–663 (1965).

17. E. C. Okress and D. M. Wroughton, "Electromagnetic Levitation of Solid and Molten Metals," J. App. Phys., **23**, 5, 545–552.

18. F. S. Grant and G. F. West, *Interpretation Theory in Applied Geophysics,* McGraw-Hill Book Co., 515–520 (1965).

19. H. Lamb, *Hydrodynamics,* Sixth Ed., Cambridge University Press (1932).

20. W. H. Reid, "The Oscillation of a Viscous Liquid Drop," Quart. App. Math. **18**, 86–89 (1960).